JCB Journal of Cell Biology

ARTICLE

Tyrosine phosphorylation of S1PR1 leads to chaperone BiP-mediated import to the endoplasmic reticulum

Mumtaz Anwar[1], Md Ruhul Amin[1], Vijay Avin Balaji Ragunathrao[1], Jacob Matsche[1], Andrei Karginov[1], Richard D. Minshall[1,2], Gary C.H. Mo[1], Yulia Komarova[1], and Dolly Mehta[1]

Cell surface G protein–coupled receptors (GPCRs), upon agonist binding, undergo serine–threonine phosphorylation, leading to either receptor recycling or degradation. Here, we show a new fate of GPCRs, exemplified by ER retention of sphingosine-1-phosphate receptor 1 (S1PR1). We show that S1P phosphorylates S1PR1 on tyrosine residue Y^{143}, which is associated with recruitment of activated BiP from the ER into the cytosol. BiP then interacts with endocytosed Y^{143}-S1PR1 and delivers it into the ER. In contrast to WT-S1PR1, which is recycled and stabilizes the endothelial barrier, phosphomimicking S1PR1 (Y^{143}D-S1PR1) is retained by BiP in the ER and increases cytosolic Ca^{2+} and disrupts barrier function. Intriguingly, a proinflammatory, but non-GPCR agonist, TNF-α, also triggered barrier-disruptive signaling by promoting S1PR1 phosphorylation on Y^{143} and its import into ER via BiP. BiP depletion restored Y^{143}D-S1PR1 expression on the endothelial cell surface and rescued canonical receptor functions. Findings identify Y^{143}-phosphorylated S1PR1 as a potential target for prevention of endothelial barrier breakdown under inflammatory conditions.

Introduction

G protein–coupled receptors (GPCRs) constitute the largest family of seven-transmembrane-spanning cell surface receptors that, upon binding to their respective ligands, stimulate heterotrimeric G proteins to rapidly trigger downstream signaling. The critical determinant of GPCR regulation of cellular function is the receptor's cell surface expression (Rosenbaum et al., 2009; Venkatakrishnan et al., 2013). Phosphorylation of GPCRs at C-terminal serine/threonine residues leads to receptor internalization by the canonical dynamin/β-arrestin–mediated pathway, following which the GPCR either recycles back to the cell surface or undergoes ubiquitin-mediated degradation (Oo et al., 2011). However, several GPCRs in the class A family, such as sphingosine-1-phosphate receptor 1 (S1PR1), contain tyrosine residues within a conserved E/DRY motif located at the boundary between transmembrane domain III and intracellular loop 2 (Cannavo et al., 2013; Rasmussen et al., 2011). Little is known about the molecular determinants of subcellular localization of tyrosine-phosphorylated GPCRs or whether the phosphorylated receptor remains functional after it is internalized.

S1PR1 is widely expressed in several organs, such as lung, brain, heart, and lymphoid glands (Cahalan et al., 2011), but its expression profile differs among endothelial cells (ECs) from various vascular beds (Cartier and Hla, 2019; Jambusaria et al., 2020). For example, S1P was shown to enhance transendothelial electrical resistance (TEER), a measure of endothelial barrier function, more so in pulmonary microvascular ECs than in pulmonary arterial ECs (Dudek et al., 2004). Single-cell RNA sequencing analysis in a mouse model of atherosclerosis also indicated that S1PR1/β-arrestin coupling and inflammatory gene expression signature differ between arterial EC subsets at vascular branch points than other EC subtypes at nonbranch points (Engelbrecht et al., 2020).

Upon binding S1P, S1PR1 transmits downstream signaling by coupling with heterotrimeric Gi protein to regulate diverse cellular functions, including maintenance of EC barrier function, as well as an effective immune response by lymphocytes (Rivera et al., 2008). S1PR1 strengthens basal EC barrier function as well as resolves lung injury by mechanisms involving intracellular Ca^{2+} ($[Ca^{2+}]_i$) transient– and Rac1/Cdcd42-GTPase–dependent cortical actin assembly, which reanneal adherens junctions (Daneshjou et al., 2015; Mehta et al., 2005; Reinhard et al., 2017). Lymphocyte-expressed S1PR1, on the other hand, regulates

[1]Department of Pharmacology, Center for Lung and Vascular Biology, College of Medicine, University of Illinois at Chicago, Chicago, IL; [2]Department of Anesthesiology, Center for Lung and Vascular Biology, College of Medicine, University of Illinois at Chicago, Chicago, IL.

Correspondence to Dolly Mehta: dmehta@uic.edu.

lymphocyte egress from secondary organs, such as spleen (Matloubian et al., 2004) and lymph nodes (Benechet et al., 2016), based on tissue S1P concentrations. Additionally, cell surface CD69 expression (Cyster and Schwab, 2012), S1PR1–C-terminal phosphorylation, and dynamin (Oo et al., 2011) regulate lymphocyte egress by internalizing S1PR1 (Willinger et al., 2015). S1PR1-deficient naive T cells thereby fail to exit the thymus and lymph nodes, leading to impaired immune response after viral infection (Baeyens et al., 2015; Matloubian et al., 2004). Thus, loss of S1PR1 function in ECs and lymphocytes is a hallmark of several vascular and chronic inflammatory diseases (Cartier and Hla, 2019; Proia and Hla, 2015).

We showed that in addition to inducing serine phosphorylation at the C-terminus, S1P also mediates S1PR1 phosphorylation on tyrosine residue Y^{143} within the ERY motif, following which the receptor is internalized but protected from degradation (Chavez et al., 2015). The Chavez et al. study raised several fundamental questions, namely: (1) How is internalized Y^{143}-S1PR1 regulated? (2) Is internalized Y^{143}-S1PR1 functional? And (3) does Y^{143}-S1PR1 function in a manner like the native receptor in terms of regulating downstream signaling? Here, we express native and phosphospecific S1PR1 mutants in ECs to assess the basis of S1PR1 phosphorylation at Y^{143} in regulating receptor localization and functions. We demonstrate a unique and functional transformation of S1PR1 when phosphorylated on Y^{143}. We show that Y^{143} phosphorylation of S1PR1 drives the receptor into the ER in a manner dependent on activation of the ER chaperone binding immunoglobulin protein (BiP). While WT-S1PR1 recycled back to the EC surface, constitutively phosphomimicking S1PR1 (Y^{143}D-S1PR1) mutant is retained in the ER by BiP and induces disruption of the endothelial barrier. The present studies have thus identified a previously unknown role of S1PR1 in destabilizing endothelial barrier function during vascular injury in a manner dependent on posttranslational modification of the receptor on Y^{143} and ER retention.

Results

Tyrosine-phosphorylated S1PR1 localizes at the ER

We cotransfected GFP-tagged WT-S1PR1, Y^{143}D-S1PR1 (phosphomimicking), or Y^{143}F-S1PR1 (phosphodefective) S1PR1 mutants along with stargazin, which fluorescently labels the plasma membrane (Inamura et al., 2006) in human umbilical vein ECs (HUVECs) to assess receptor localization. Using total internal reflection fluorescence (TIRF) microscopy, which detects fluorescence within 100 nm from the cell surface and thus detects plasma membrane localization of receptor (Doronzo et al., 2019), as well as confocal microscopy, we observed the predicted colocalization of WT-S1PR1 and Y^{143}F-S1PR1 with stargazin (Fig. 1, A and B; and Fig. S1, A and B). However, Y^{143}D-S1PR1 failed to colocalize with stargazin and, rather, was found localized in an intracellular compartment (Fig. 1, A and B; and Fig. S1, A and B) distinct from the nucleus (Fig. S1, A and B).

The ER regulates trafficking of newly synthesized or posttranslationally modified GPCRs (Drake et al., 2006). We therefore overexpressed WT-, Y^{143}D-, and Y^{143}F-S1PR1 mutants with an mCherry-tagged ER cDNA to test the possibility that S1PR1 traffics to the ER upon tyrosine phosphorylation. The ER-mCherry cDNA has a calreticulin signal sequence at the N-terminus that directs insertion into the ER and a KDEL coding sequence at the C-terminus that is responsible for retention in the ER (Dickens et al., 2016). Interestingly, we found that Y^{143}D-S1PR1 colocalized with ER-mCherry, while WT-S1PR1 or Y^{143}F-S1PR1 did not (Fig. 1, C and D).

We then stimulated ECs transducing WT-S1PR1 or Y^{143}F-S1PR1 with S1P to assess the time course of S1PR1 trafficking to the ER. We found that WT-S1PR1 localized to the ER within 2.5 min and remained there for up to 5 min, returning to the cell surface up to 20 min later. In contrast, Y^{143}F-S1PR1 did not internalize at all, even after S1P stimulation (Fig. 2, A and B). S1P had no effect on Y^{143}D-S1PR1 internalized localization (data not shown).

To address whether ER localization of GFP-S1PR1 is not the result of cleavage of GFP from S1PR1 or Y^{143}D-S1PR1, we tagged WT-S1PR1 or Y^{143}D-S1PR1 with the photoswitchable fluorescent protein Dendra2, which exhibits a shift in emission spectrum from a 488- to 561-nm maximum wavelength after photoconversion (Chudakov et al., 2007). We irradiated Dendra2 and monitored S1PR1 dynamics with or without S1P stimulation. We observed in unstimulated ECs that S1PR1-Dendra2 remained at the cell surface even after photoconversion (Fig. 2, C and D). However, S1P addition rapidly increased S1PR1-Dendra2 inside the cell, demonstrating S1PR1 internalization (Fig. 2, C–E). In line with this, we also observed that Y^{143}D-S1PR1-Dendra2 remained internalized with or without S1P stimulation following photoconversion (Fig. S1, C and D). These findings demonstrate that upon tyrosine phosphorylation at Y^{143}, the receptor is trafficked back from the ER to the EC surface. Consistently, the Y^{143}D-S1PR1 mutant was constitutively internalized and localized in the ER.

GPCRs homo- and hetero-oligomerize (Ramsay et al., 2002). Previously, we showed that Y^{143}D-S1PR1 mutant expression in naive or S1PR1-depleted ECs disrupts barrier function (Chavez et al., 2015), raising the possibility that the overexpression of mutated S1PR1 may affect the localization and function of endogenous S1PR1. Thus, we coexpressed GFP-tagged WT-S1PR1 with vector, HA-tagged Y^{143}D-S1PR1, or HA-tagged Y^{143}F-S1PR1 mutants and determined whether S1PR1 mutants compromise GFP localization. We found that GFP-tagged S1PR1 is internalized in ECs when cotransduced with HA-tagged Y^{143}D-S1PR1. However, GFP-tagged S1PR1 remained at the EC surface in ECs cotransducing vector and HA-tagged Y^{143}F-S1PR1 mutant (Fig. 3, A and B). We also measured TEER in ECs transducing WT-S1PR1-GFP along with HA-tagged Y^{143}F- or Y^{143}D-S1PR1 mutants, respectively. Consistent with previous findings, we observed that Y^{143}D-S1PR1 disrupted barrier function basally, which was not reversed even after S1P addition (Fig. 3, C and D). This response was not seen in ECs cotransfected with WT-S1PR1-GFP and HA-tagged Y^{143}F-S1PR1 mutant. Altogether, these findings demonstrate that Y^{143}D-S1PR1 serves as a dominant negative for endogenous S1PR1 and thereby disrupts EC barrier function.

Dynamin pinches off the phosphorylated receptor

Dynamin plays a critical role in endocytosis of GPCRs in a GTP-dependent manner (Ferguson and De Camilli, 2012). To assess the possibility that Y^{143}-phosphorylated S1PR1 was initially expressed on the cell surface and then internalized in a dynamin-dependent

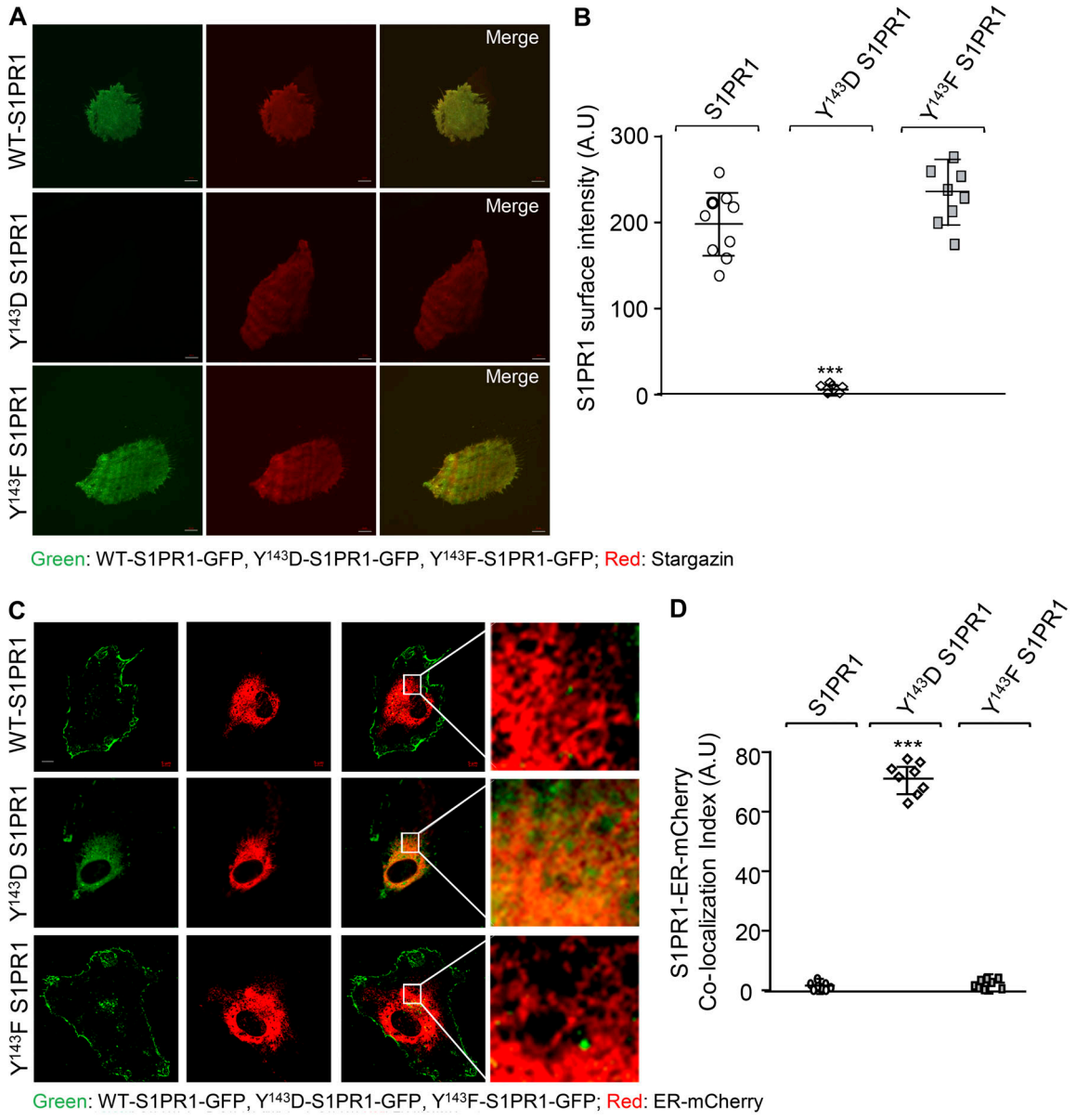

Figure 1. **Tyrosine-phosphorylated S1PR1 traffics to the ER. (A)** TIRF images of WT-S1PR1, $Y^{143}F$-S1PR1, and $Y^{143}D$-S1PR1 mutants with stargazin taken at 100× magnification. Scale bars, 10 µm. **(B)** Quantification of the surface expression of S1PR1. *n* = 7–9 cells/group from experiments repeated three times. **(C)** Confocal images of S1PR1 and ER-mCherry taken at 63× magnification. Inset: 5× magnified image of the area in rectangle. Scale bar, 5 µm and 25 µm in insets. **(D)** Quantification of the percent colocalization of the S1PR1 with ER-mCherry. *n* = 7–10 cells/group from experiments repeated three times. Data in B and D are shown as mean ± SD. ***, P < 0.0001 compared with WT and $Y^{143}F$-S1PR1 by one-way ANOVA with two-tailed paired *t* test. See also Fig. S1, A and B. A.U, arbitrary units.

manner, we treated ECs transducing S1PR1 mutants with dynasore, a specific small-molecule inhibitor of dynamin (Macia et al., 2006), or depleted dynamin using siRNA. Biotinylation assay showed that compared with WT-S1PR1 or $Y^{143}F$-S1PR1, cell surface expression of $Y^{143}D$-S1PR1 was reduced by ∼90% (Fig. 4, A and B). Dynasore treatment restored $Y^{143}D$-S1PR1 cell surface expression to the level observed in ECs transducing WT-S1PR1 or $Y^{143}F$-S1PR1 (Fig. 4, A and B). Similar results were obtained in dynamin-depleted ECs (Fig. 4, C and D).

Mutation of Lys 44 to Ala (K44A) in dynamin impairs its GTPase activity and thereby inhibits receptor endocytosis (Damke et al., 2001). Thus, in other studies, we cotransduced ECs with K44A-mCherry-dynamin along with either GFP-tagged WT-S1PR1, $Y^{143}D$-S1PR1, or $Y^{143}F$-S1PR1 and assessed S1PR1 cell surface expression by confocal microscopy. Overexpression of GTPase-dead dynamin restored $Y^{143}D$-S1PR1 expression on the EC surface (Fig. 4, E and F), demonstrating that dynamin promotes internalization of $Y^{143}D$-S1PR1 in a manner consistent with dynamin-dependent regulation of GPCR trafficking (Willinger et al., 2014).

Rab-GTPases contribute to many steps in vesicular trafficking, including endocytosis and sorting to subcellular compartments

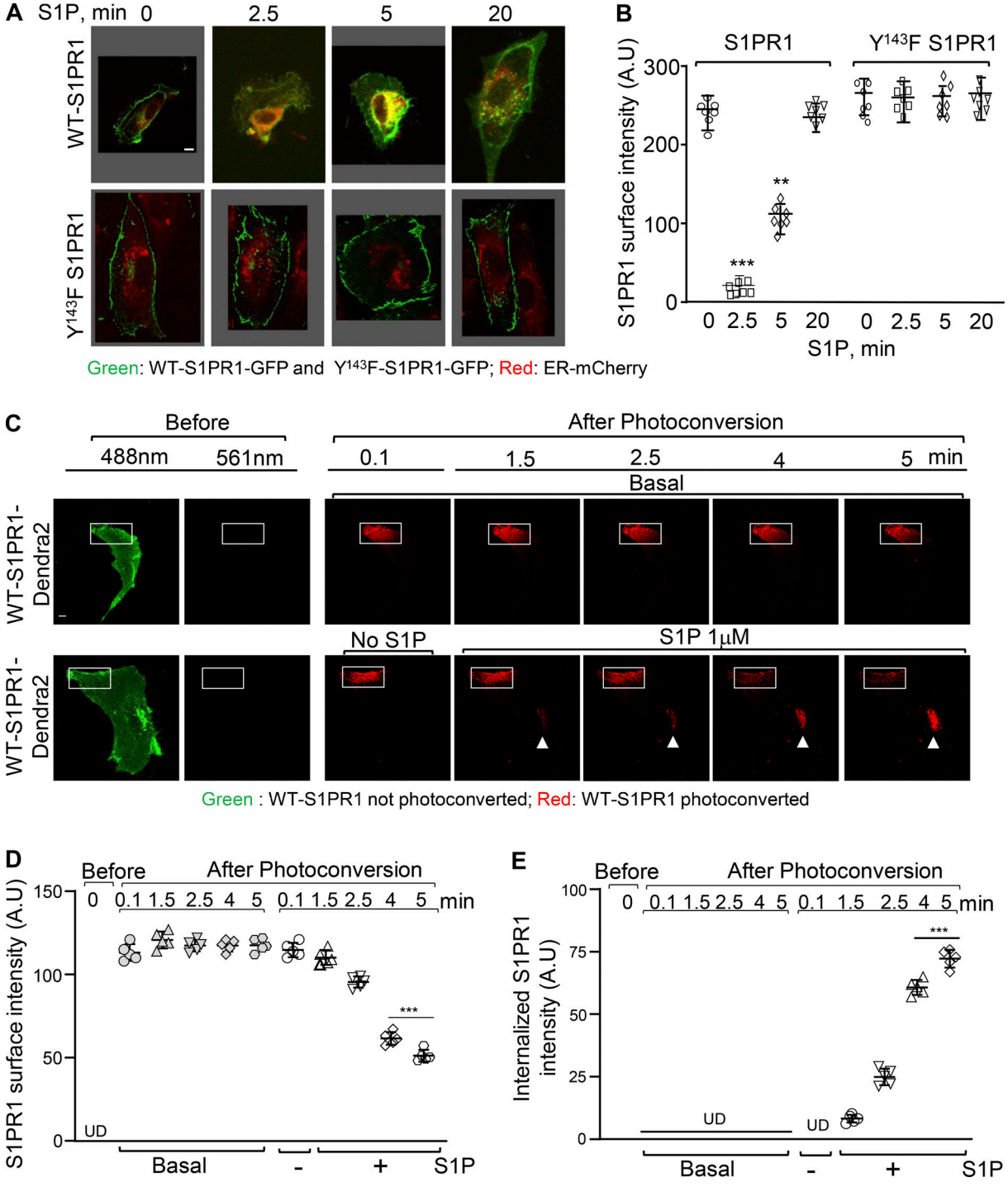

Figure 2. **Dynamics of the tyrosine-phosphorylated S1PR1 to the ER. (A)** Confocal images of S1PR1 and ER (mCherry) without or with S1P (1 μM). Gray background indicates the area outside the image. Scale bar, 5 μm. **(B)** Quantification of the surface expression. *n* = 5–7 cells/group from experiments repeated three times. One-way ANOVA with paired two tailed *t* test. **, P < 0.001; ***, P < 0.0001 compared with WT-S1PR1 at 0 and 20 min and Y^{143}F-S1PR1 at 0, 2.5, 5, and 20 min. **(C)** Time-lapse images of S1PR1–Dendra2 before and after photoconversion at time 0 (indicated by green, rectangles) and after the addition of S1P (1 μM; red, rectangles). 488-nm channel (green) = unconverted S1PR1; 561-nm channel (red) = photoconverted S1PR1. Scale bar, 10 μm. **(D and E)** Quantification using images in C. *n* = 5–6 cells from experiments repeated two times. **(D and E)** One-way ANOVA with paired two tailed *t* test. ***, P < 0.0001 compared with WT-S1PR1-Dendra2 at basal levels or after S1P stimulation at 2.5 min (D) or at 1.5 min (E). Data in B, D, and E are shown as mean ± SD. See also Fig. S1, C and D. A.U, arbitrary units; UD, undetectable.

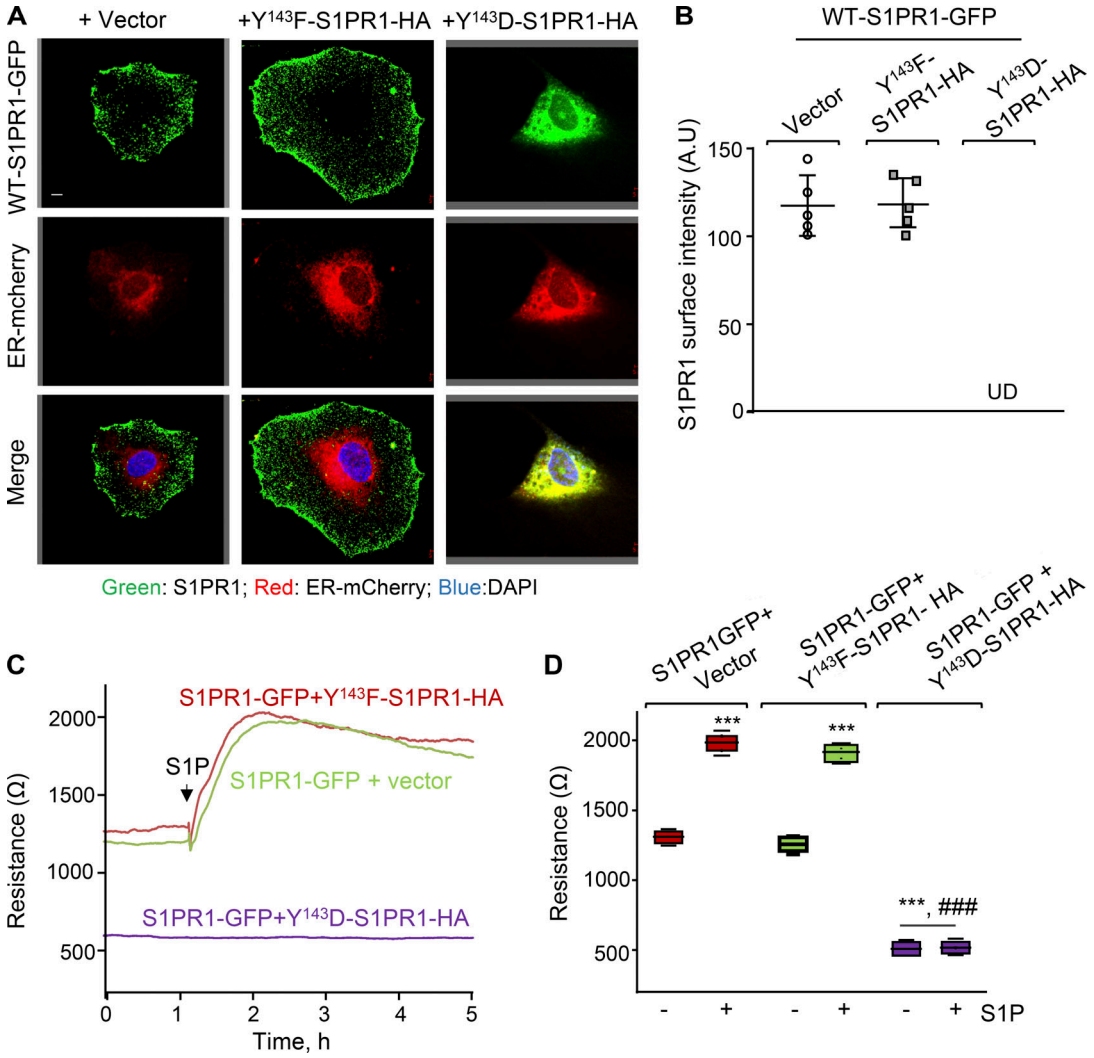

Figure 3. **Phosphorylated S1PR1 internalizes endogenous S1PR1. (A)** Confocal image at 63× magnification from HUVECs coexpressing GFP-WT-S1PR1 and ER-mCherry along with HA-tagged vector or HA-Y^{143}F- or HA-Y^{143}D-S1PR1 mutants. Scale bar, 5 µm. **(B)** Quantification of the S1PR1 surface intensity using images in A. *n* = 5–6 cells/group from experiments repeated two times. **(C)** TEER trace in ECs coexpressing WT-S1PR1-GFP and HA-tagged vector or S1PR1 mutants. **(D)** Mean ± SD of TEER using multiple traces in C. Basal TEER (–) = values between 10 and 30 min; S1P-stimulated TEER (+) = values between 2 and 2.5 h. **(D)** One-way ANOVA with paired two tailed *t* test. ***, P < 0.0001 compared with unstimulated cells; ###, P < 0.0001 compared with S1P-stimulated WT-S1PR1 + vector or HA-Y^{143}F-S1PR1. A.U, arbitrary units; UD, undetectable.

(Hutagalung and Novick, 2011). We therefore assessed whether Rab-GTPases regulate S1PR1 trafficking to the ER. ECs primarily express Rab5, 7, 9, and 11 (Chichger et al., 2016), and previous studies showed that Rab5 and Rab7 are involved in regulating protein sorting and recycling to early endosomes (de Renzis et al., 2002; Gorvel et al., 1991). Thus, we depleted Rab5 and Rab7 and found that their depletion had no effect on S1P-mediated trafficking of WT-S1PR1 to the ER (Fig. S2, A–D). Also, the Y^{143}D-S1PR1 mutant remained localized at the ER in control or Rab-depleted ECs (data not shown), ruling out the role of these Rab-GTPases in trafficking S1PR1 to the ER.

Y^{143}-phosphorylated S1PR1 interacts with BiP

We previously showed that S1P maximally phosphorylates S1PR1 at Y^{143} within 5 min, leading to receptor internalization followed by receptor dephosphorylation and reappearance on the EC surface between 15 and 20 min (Chavez et al., 2015). We next harvested lysates from ECs overexpressing WT-S1PR1 at 5 min (maximal phosphorylation) or 15 min (dephosphorylated) after S1P stimulation and performed mass spectrometry of the immunocomplex to identify possible binding partners for tyrosine-phosphorylated S1PR1 (Y^{143}-S1PR1). In parallel, we also used lysates from unstimulated Y^{143}D-S1PR1– or Y^{143}F-S1PR1–expressing ECs. We specifically focused on binding partners that may affect S1PR1 retention in the ER and identified BiP (also known as GPR78) as the key interacting partner for phosphorylated S1PR1 (Fig. S3, A–E). We confirmed this interaction using immunoprecipitation studies in which BiP coprecipitated with WT-S1PR1 at 5 min, whereas the interaction was not detected at 15 min (Fig. 5, A and B). BiP interacted with the Y^{143}D-S1PR1 mutant constitutively, and the interaction was not altered after addition of S1P (Fig. 5, A–D). However, BiP failed to interact with

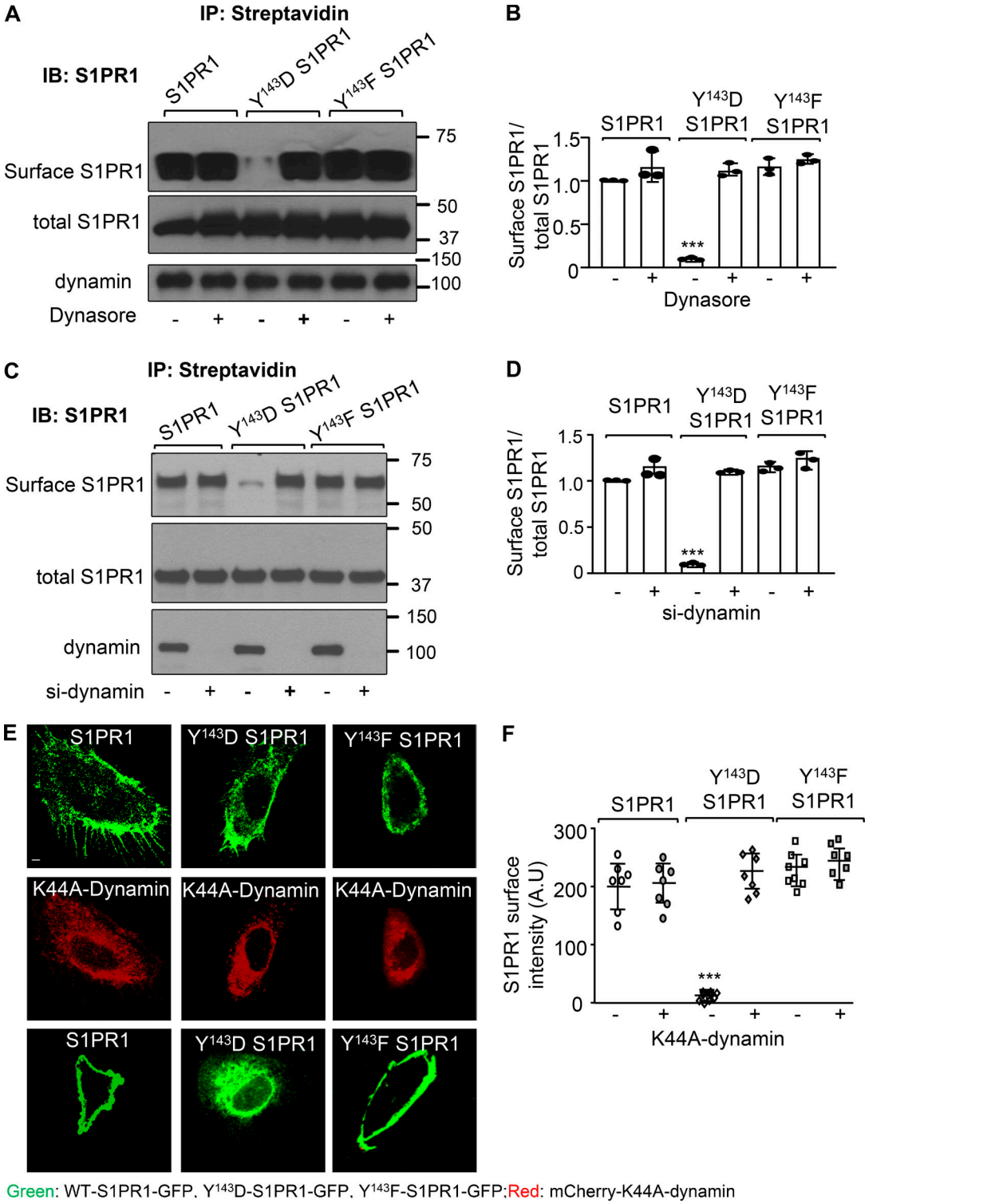

Figure 4. **Dynamin internalizes tyrosine-phosphorylated S1PR1. (A)** S1PR1 surface expression without (–) or with (+) dynasore (100 µM) determined using anti-S1PR1 antibody. ECs were first transfected with indicated cDNAs. Dynasore was added within 30 min after transfection, and cells were lysed after 24 h. Total S1PR1 and dynamin expression were quantified using anti-S1PR1 or anti-dynamin antibodies. **(B)** Densitometry of S1PR1 surface expression over total S1PR1 using blots in A. *n* = 3 independent experiments. **(C)** S1PR1 surface expression in ECs transfected with control siRNA (–) or dynamin siRNA (+) determined as in A. **(D)** Densitometry quantified as in B. *n* = 3 independent experiments. **(E)** Confocal images showing S1PR1 cell surface localization following co-transfection with mCherry-tagged GTPase-defective dynamin (K44A-dynamin). Scale bar, 5 µm. **(F)** Quantification of S1PR1 cell surface expression. *n* = 5–8 cells/group from experiments repeated three times. All data in B, D, and F are shown as mean ± SD. One-way ANOVA with paired two tailed *t* test. ***, P < 0.0001 compared with WT-S1PR1 or Y^{143}F-S1PR1. See also Fig. S2, A–D. A.U, arbitrary units; IB, immunoblot; IP, immunoprecipitation. **(A and C)** Molecular weight marker in kD.

the Y^{143}F-S1PR1 mutant, even after S1P stimulation (Fig. 5, C and D). Imaging studies similarly showed that BiP colocalized with WT-S1PR1 within 5 min of S1P stimulation but not at 15 min. In contrast to the Y^{143}F-S1PR1 mutant, the Y^{143}D-S1PR1 mutant consistently colocalized with BiP at the ER without or with S1P stimulation (Fig. 5, E and F). These findings suggest that Y^{143} phosphorylation plays a key role in mediating BiP interaction with S1PR1.

ER-localized phosphorylated S1PR1 induces Ca^{2+} signaling in a Gi-dependent manner

S1P increases $[Ca^{2+}]_i$ in a Gi-dependent manner (Li et al., 2015; Mehta et al., 2005). Thus, we addressed the possibility that S1PR1 phosphorylation mediates an increase in $[Ca^{2+}]_i$ level in response to S1P in ECs transducing WT-S1PR1, Y^{143}D-S1PR1, or Y^{143}F-S1PR1. ECs were incubated with the Ca^{2+}-sensitive dye Fura-2 AM for 15 min, after which the cells were rinsed and $[Ca^{2+}]_i$ determined in GFP-expressing ECs (Yazbeck et al., 2017). As expected, S1P increased $[Ca^{2+}]_i$ in ECs transducing WT-S1PR1 or the Y^{143}D-S1PR1 mutant but only modestly in ECs transducing Y^{143}F-S1PR1. However, S1P-induced increase in $[Ca^{2+}]_i$ was 3.5-fold higher in ECs transducing the Y^{143}D-S1PR1 mutant than ECs expressing WT-S1PR1 or the Y^{143}F-S1PR1 mutant (Fig. 6, A and B). These findings indicate that ER-retained Y^{143}D-S1PR1 mutant is functional, while the Y^{143}F-S1PR1 mutant largely prevents the increase in cytosolic Ca^{2+}.

We next inhibited Gi using pertussis toxin (PTX; Gunther et al., 2000) to address its role in regulating the increase in $[Ca^{2+}]_i$. Intriguingly, S1P failed to increase $[Ca^{2+}]_i$ in PTX-pretreated ECs transducing WT-, Y^{143}D-, or Y^{143}F-S1PR1 mutant (Fig. 6, C and D). We also transfected these mutants into human embryonic kidney (HEK) cells as they do not express the S1PR1 receptor (Balaji Ragunathrao et al., 2019) and similarly found that Y^{143}D-S1PR1 augmented $[Ca^{2+}]_i$ in a Gi-dependent manner (Fig. S4, A and B). In other studies, we performed coimmunoprecipitation experiments using lysates from ECs expressing WT or mutated receptor to address the possibility that Y^{143}D-S1PR1 forms a complex with Gi. We found that Y^{143}D-S1PR1 pulled down Gi to the same level as S1PR1 or Y^{143}F-S1PR1 (Fig. 6, E and F). Thus, these findings indicate that phosphorylated S1PR1 traffics to the ER and induces $[Ca^{2+}]_i$ mobilization in a Gi-dependent manner.

S1P may increase the $[Ca^{2+}]_i$ concentration by mobilizing the release of Ca^{2+} from ER stores and subsequently activating Ca^{2+} entry through nonselective cation channels (Mehta and Malik, 2006). Thus, we addressed the role of each of these components in enhancing $[Ca^{2+}]_i$ in ECs expressing WT or mutated S1PR1. We separated the two phases of the Ca^{2+} transient ER-Ca^{2+} release and store-operated Ca^{2+} entry (SOCE) mediated by plasmalemmal Ca^{2+} channels (Mehta et al., 2005; Yazbeck et al., 2017) by stimulating the cells under Ca^{2+}-free bath conditions to deplete the ER-Ca^{2+} store followed by add back of Ca^{2+} to monitor SOCE. ECs transducing the Y^{143}D-S1PR1 mutant showed markedly increased SOCE in response to S1P compared with WT-S1PR1–expressing cells (Fig. 6, G and H). ECs expressing Y^{143}F-S1PR1 showed negligible SOCE.

We next depleted BiP to assess its causal role in trapping S1PR1 in the ER and inducing SOCE. We found that siRNA depleted BiP to undetectable levels between 24 and 72 h (Fig. S5, A and B). We then cotransfected ECs with WT- or Y^{143}D-S1PR1 along with scrambled (siSC) or BiP siRNA, and after 36 h, S1PR1 cell surface localization was determined using TIRF. Whereas BiP depletion had no effect on WT-S1PR1 cell surface expression, depletion of BiP restored Y^{143}D-S1PR1 expression on the EC surface (Fig. 7, A and B). Intriguingly, depletion of BiP prevented SOCE in both WT-S1PR1– and Y^{143}D-S1PR1–transducing ECs (Fig. 7, C and D). Thus, BiP was responsible for retention of the Y^{143}-phosphorylated receptor in the ER and for augmented Ca^{2+} levels induced by S1P stimulation (Fig. 7, C and D).

To determine whether BiP and Gi were responsible for decreasing endothelial permeability in the Y^{143}D-S1PR1 mutant–expressing ECs shown above, we determined TEER in BiP-depleted ECs transducing WT-S1PR1 or Y^{143}D-S1PR1. We also inhibited Gi using PTX, as above. Inhibition of Gi failed to alter barrier disruption by the mutant (Fig. S4, C and D). However, depletion of BiP restored basal TEER in ECs transducing the Y^{143}D-S1PR1 mutant. Furthermore, addition of S1P enhanced TEER in ECs transducing the Y^{143}D-S1PR1 mutant after BiP depletion to a level like EC-expressing WT-S1PR1 (Fig. 7, E and F), thus suggesting that phosphorylated S1PR1, through its interaction with BiP, switches its barrier-enhancing function to a disruptive one.

BiP translocates to cytosol and binds S1PR1 through its ATPase domain

While BiP is known to be an ER-localized chaperone, it is detected in the nucleus, mitochondria, and cytosol (Ni et al., 2011). The BiP ATPase domain (aa 28–405), substrate-binding domain (SBD; aa 422–651), and KDEL motif (aa 651–654) regulate BiP chaperone function (Carrara et al., 2015). To test the possibility that S1P induces BiP recruitment to the cytosol to facilitate BiP interaction with endocytosed S1PR1, we assessed alterations in BiP localization and ATPase activity following S1P stimulation of ECs. We also mapped the domain in BiP that binds phosphorylated S1PR1.

Using cell fractionation and imaging, we assessed alteration in cellular localization of BiP following S1P stimulation. We found that S1P increased BiP translocation to the cytosolic fraction within 2.5–5 min, which was no longer apparent at 15 min (Fig. 8, A and B). Similarly, imaging studies showed that S1P induced recruitment of BiP from the ER to the cytosol within 2.5–5 min (Fig. 8, C and D). Interestingly, S1P also increased BiP-ATPase activity (Fig. 8 E) coinciding with S1PR1 interaction with BiP (Fig. 5, E and F).

To map the domain via which BiP binds S1PR1, we cotransduced HA-tagged vector, full-length BiP, BiP containing only the ATPase domain (BiP-ATPase), and BiP containing the SBD (BiP-SBD) along with the GFP-tagged Y^{143}D-S1PR1 mutant in ECs (Fig. 8 F). Coimmunoprecipitation studies showed that phosphorylated S1PR1 interacted with BiP through its ATPase domain (Fig. 8, G and H). In addition, ECs expressing Y^{143}D-S1PR1 showed an approximately eightfold increase in BiP-ATPase activity above EC-expressing WT-S1PR1 (Fig. 8 I). These data indicate that S1P initiates two events in parallel: S1P phosphorylates S1PR1 at Y^{143} and promotes the translocation of BiP to the cytosol,

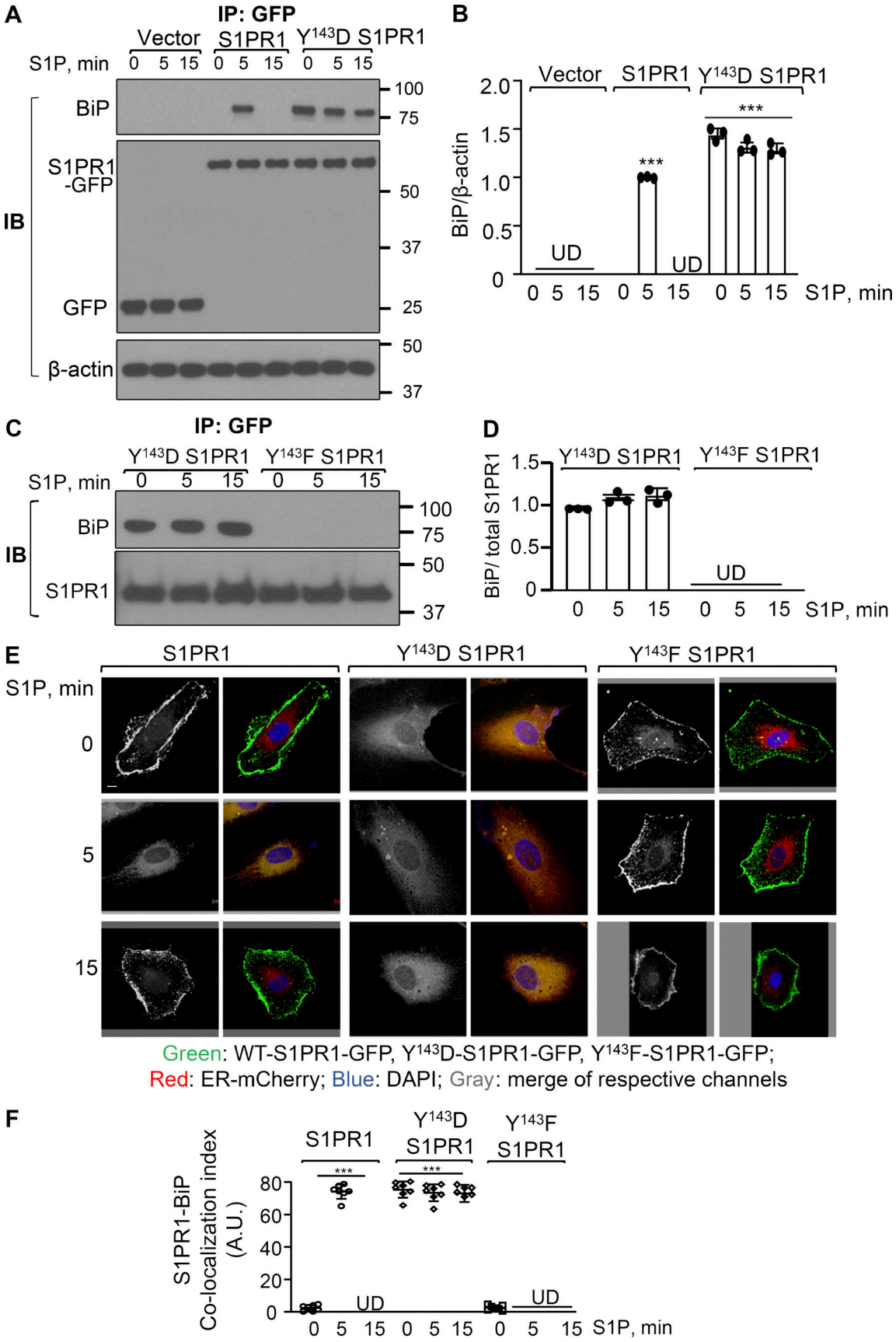

Figure 5. **Phosphorylated S1PR1 interacts with BiP. (A)** Pulldown of BiP from HUVEC transducing vector, GFP-S1PR1, or GFP-Y^{143}D-S1PR1 after S1P stimulation at indicated times. Anti-GFP antibody was used to pull down; immunocomplexes were probed with anti-BiP antibody to assess interaction. Anti-GFP

or anti-β-actin antibody was used to confirm total protein. **(B)** Mean ± SD of BiP interaction with S1PR1 using blots in A and with β-actin as loading control. $n = 3$ independent experiments. ***, $P < 0.0001$ compared with unstimulated WT-S1PR1 by one-way ANOVA with two-tailed paired t test. **(C)** Pulldown of BiP from ECs expressing GFP-Y^{143}F- or GFP-Y^{143}D-S1PR1 mutants processed as in A. **(D)** Mean ± SD of the BiP interaction with S1PR1 normalized using total S1PR1. $n = 3$ independent experiments. **(E)** Confocal images illustrating colocalization of S1PR1 with BiP without or with S1P stimulation. Cells were also stained for DAPI to assess nuclei. Gray background indicates the area outside the image. Scale bar, 5 µm. **(F)** Quantitation of the colocalization index plotted as mean ± SD. ***, $P < 0.0001$ compared with unstimulated WT-S1PR1 or Y^{143}F-S1PR1 by one-way ANOVA with two-tailed paired t test. See also Fig. S3, A–E. A.U., arbitrary units; IB, immunoblot; IP, immunoprecipitation; UD, undetectable. **(A and C)** Molecular weight marker in kD.

leading to increase in BiP-ATPase activity, thereby augmenting its chaperone function and enabling BiP to retain Y^{143}D-S1PR1 in the ER.

TNF-α disrupts barrier function by inducing S1PR1 Y^{143} phosphorylation and ER localization

The proinflammatory cytokine TNF-α released during tissue injury disrupts endothelial barrier function by inducing protein phosphorylation and augmenting SOCE (Vandenbroucke et al., 2008). We therefore surmised that increased S1PR1 phosphorylation at Y^{143} may be a common mechanism by which inflammatory mediators, such as TNF-α, disrupt barrier function. Hence, we stimulated ECs with TNF-α for the indicated times and determined S1PR1 phosphorylation on Y^{143}. We found that TNF-α induced a fivefold increase in S1PR1 tyrosine phosphorylation within 15 min. Receptor phosphorylation persisted at this level for up to 60 min (Fig. 9, A and B). However, TNF-α did not induce phosphorylation in ECs transducing Y^{143}F-S1PR1 (Fig. S5, C and D). In these experiments, we also determined whether the TNF-α–induced increase in S1PR1 phosphorylation enhanced S1PR1's interaction with BiP. We found that TNF-α induced BiP interaction with S1PR1 in a manner dependent on phosphorylation of the Y^{143} residue (Fig. 9, A and B). TNF-α also rapidly induced receptor internalization (Fig. 9, C and D) and disrupted basal barrier function in ECs, which was not rescued by addition of S1P (Fig. 9, E and F). Intriguingly, TNF-α failed to disrupt barrier function in BiP-depleted ECs (Fig. 9, G and H). These results demonstrate that phosphorylation of S1PR1 at Y^{143} and interaction with BiP play a key role in disrupting barrier function under inflammatory conditions.

Discussion

Here, we identify the unique role of S1PR1 Y^{143} phosphorylation in promoting S1PR1 interaction with BiP. BiP in turn translocates Y^{143}-S1PR1 to the ER for mediating SOCE and barrier disruption. We show that in response to S1P, the transient nature of S1PR1 phosphorylation at Y^{143} results in rapid internalization of the receptor to ER by BiP followed by receptor reappearance at the cell surface in the next 20 min. However, the non-GPCR agonist TNF-α, by inducing long-lasting phosphorylation of S1PR1 at Y^{143}, sustained S1PR1 interaction with BiP at the ER, causing it to disrupt barrier function. We recapitulated these findings using Y^{143}D-S1PR1 and Y^{143}F-S1PR1 mutants. We show that unlike WT-S1PR1 or Y^{143}F-S1PR1, BiP trapped Y^{143}D-S1PR1 in the ER, which led to amplified SOCE and barrier disruption.

The large GTPase dynamin plays a critical role in the internalization and trafficking of GPCRs (Ferguson and De Camilli, 2012). Additionally, dynamin GTPase activity is required for maintaining the activity of internalized S1PR1 required for egress of T lymphocytes from lymphoid and thymus tissues (Benechet et al., 2016; Matloubian et al., 2004). Thus, we focused on dynamin in regulating the fate of phosphoreceptors within ECs. We showed that depletion of dynamin or transduction of GTPase-defective (K44A) dynamin mutant restored Y^{143}D-S1PR1 mutant expression on the cell surface, indicating that the Y^{143}D-S1PR1 mutant was not degraded but constitutively internalized in a dynamin-dependent manner.

That S1P induces internalization of S1PR1 was known (Anwar and Mehta, 2020). However, the questions of how Y^{143} phosphorylated S1PR1 was shielded from degradation and whether phosphorylation of S1PR1 at Y^{143} was a general mechanism to compromise the EC barrier during inflammation were unknown. Our results defined a novel role of tyrosine phosphorylation of S1PR1 in favoring its localization to a specific organelle in a spatially and temporally defined manner. We showed that WT-S1PR1, upon binding S1P, transiently localized to the ER where it interacted with BiP to induce physiologically relevant Ca^{2+} signaling. The transient nature of this Ca^{2+} signaling might be explained by the activity of PTP1B, a tyrosine phosphatase that resides in the ER (Haj et al., 2002). A plausible scenario consistent with our experimental observations is that PTP1B dephosphorylates Y^{143}-phosphorylated S1PR1, thereby disrupting its interaction with BiP, leading to reexpression of WT-S1PR1 on the cell surface. In support of this conclusion, we showed that Y^{143}D-S1PR1 mutant remained in the ER and disrupted barrier function while the Y^{143}F-S1PR1 mutant remained on the cell surface. We also showed that TNF-α, a potent inflammatory cytokine released during diverse vascular inflammatory conditions and known to induce cSrc activity and inhibit tyrosine phosphatases (DeLalio et al., 2019), promoted the phosphorylation of S1PR1 on Y^{143}. Unlike S1P, phosphorylation induced by TNF-α was sustained, leading to retention of the phosphorylated receptor in the ER followed by barrier disruption. Hence, in the case of TNF-α, it is possible that altered phosphatase activity, together with increased cSrc activity, led to long-lasting internalization of the receptor and barrier disruption.

ER store depletion is needed for activation of SOCE, which then induces EC contraction and disrupts EC barrier function by mechanisms involving suppression of Rac1 activity by RhoA (Komarova et al., 2017). Previously, we showed that while Gi inhibited both ER Ca^{2+} release and SOCE following S1P ligation of S1PR1, barrier enhancement by the receptor only required ER Ca^{2+} release (Mehta et al., 2005). Thus, inhibition of Gi is predicted to prevent ER Ca^{2+} release as well as SOCE and endothelial barrier enhancement induced by S1PR1 expressed on the cell surface. In line with this, we show that S1P markedly augmented Ca^{2+} entry (SOCE) in ECs as well as in HEK cells transducing

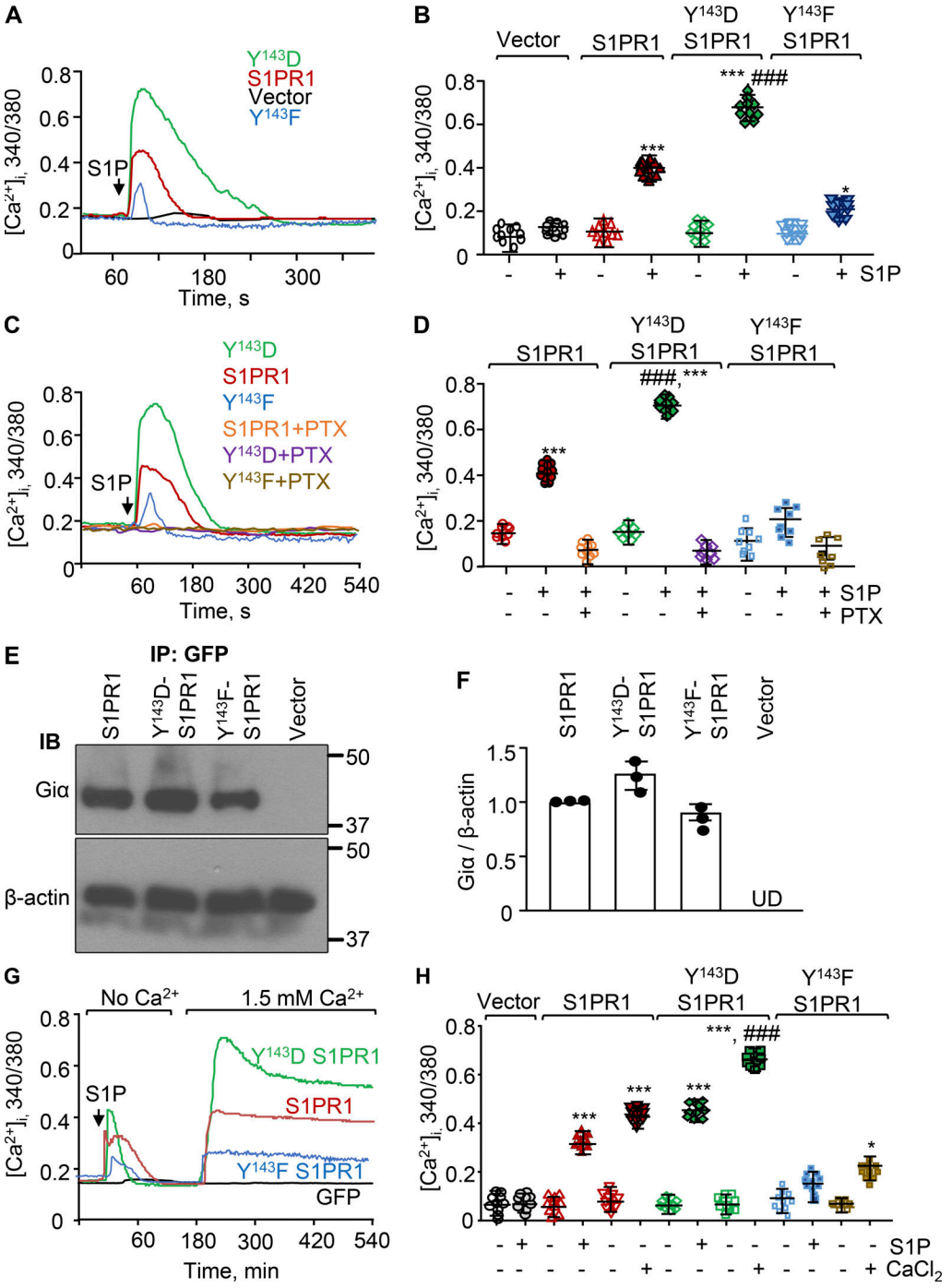

Figure 6. **$Y^{143}D$-S1PR1 augments $[Ca^{2+}]_i$ in a Gi-dependent manner. (A)** Traces showing increase in $[Ca^{2+}]_i$ in response to 1 µM S1P from HUVEC transducing vector, GFP-WT-S1PR1, GFP-$Y^{143}F$-, or GFP-$Y^{143}D$-S1PR1 mutants. **(B)** Mean ± SD of $[Ca^{2+}]_i$ from 6–10 cells in a field from experiments repeated multiple times. Basal Ca^{2+} (–) analyzed at 45 s; peak increase in Ca^{2+} analyzed at 90 s. ***, P < 0.0001 compared with unstimulated vector or WT-S1PR1; ###, P < 0.0001 compared with S1P-stimulated WT-S1PR1 by one-way ANOVA with two-tailed paired *t* test. **(C)** $[Ca^{2+}]_i$ (+) in response to 1 µM S1P from ECs expressing cDNA as in A after pretreatment with PTX (50 µM) for 2 h. **(D)** Mean ± SD of $[Ca^{2+}]_i$ from 6–10 cells in a field from experiments repeated multiple times. Basal Ca^{2+} (–) analyzed at 45 s; peak increase in Ca^{2+} analyzed at 90 s. ***, P < 0.0001 compared with unstimulated vector or WT-S1PR1; ###, P < 0.0001 compared with S1P-stimulated WT-S1PR1 by one-way ANOVA with two-tailed paired *t* test. **(E)** Pulldown of Gi with S1PR1 from ECs expressing vector or S1PR1 cDNA as in A. Anti-GFP antibody was used for pulldown. Immunocomplexes were probed using anti-Giα antibody. β-Actin was used as a loading control. **(F)** Densitometry of Giα normalized against β-actin. Experiments were repeated three times independently. **(G)** ER Ca^{2+} release versus SOCE from ECs transducing cDNAs as in A. ECs bathed in Ca^{2+}-free medium were stimulated with 1 µM S1P to determine Ca^{2+} release (first peak). After Ca^{2+} declined to basal level, 1.5 mM Ca^{2+} was readded to induce SOCE. **(H)** Mean ± SD of $[Ca^{2+}]_i$ (*n* = 7–10 cells/group) from experiments repeated three times. Basal Ca^{2+} (–) was analyzed at 20 s; peak increase in Ca^{2+} from the ER was analyzed at 45 s, while peak of SOCE was analyzed 210 s. *, P < 0.05; ***, P < 0.0001 compared with unstimulated vector or WT-S1PR1; ###, P < 0.0001 compared with WT-S1PR1 after S1P stimulation by one-way ANOVA with two-tailed paired *t* test. See also Fig. S4, A and B. IB, immunoblot; IP, immunoprecipitation; UD, undetectable. **(E)** Molecular weight marker in kD.

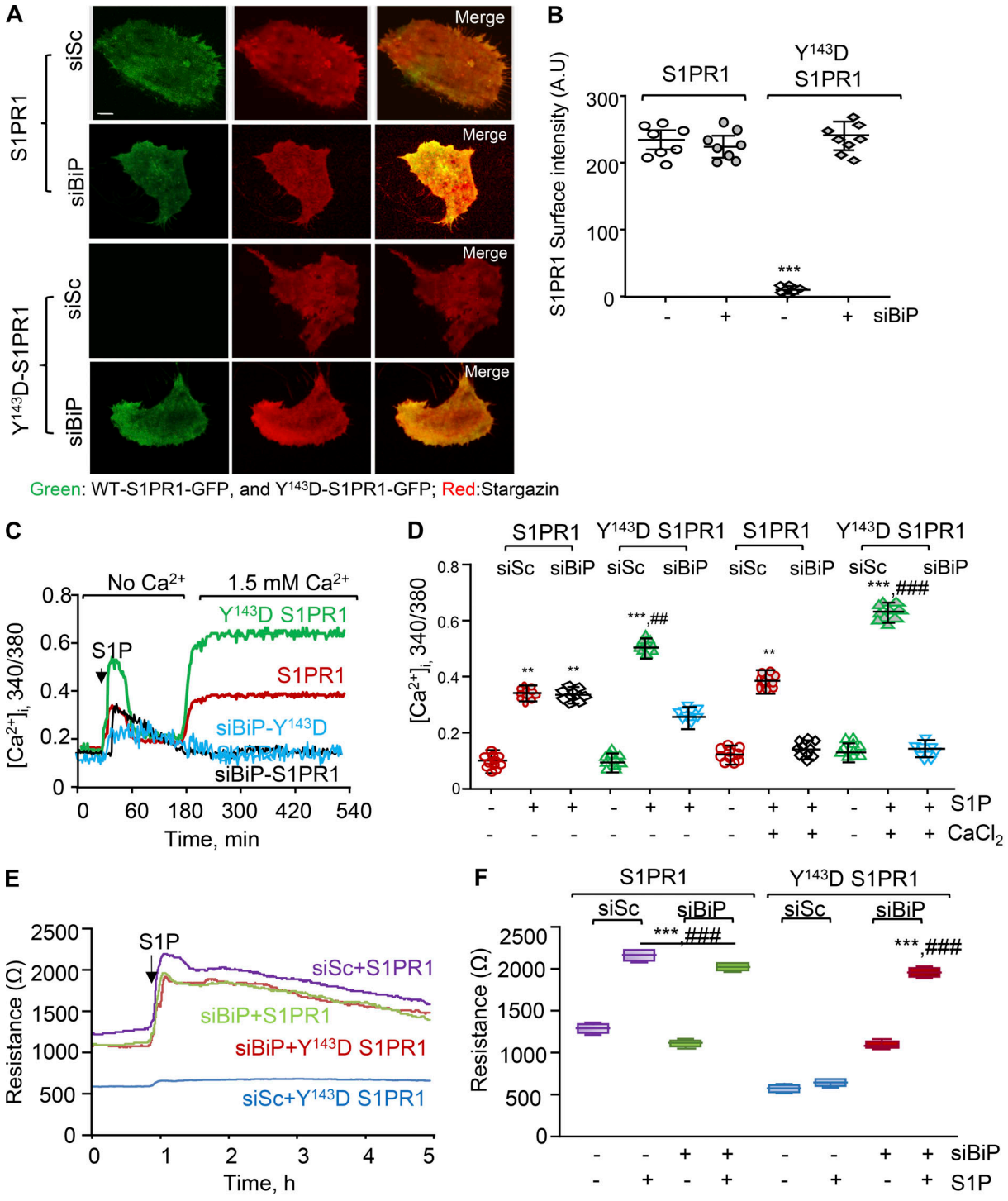

Figure 7. **Depletion of BiP restores Y143D-S1PR1 cell surface localization and endothelial barrier function. (A)** Live cell TIRF images taken at 100× magnification from control siRNA (siSc) or BiP-depleted (siBiP) ECs transducing WT- or Y143D-S1PR1. ECs were first transfected with siRNA and at 24 h and retransfected with indicated S1PR1 cDNA, and images were acquired after 48 h. Scale bar, 10 µm. **(B)** Quantification of S1PR1 surface expression (n = 7–10 cells/group) from experiments performed three times independently. ***, P < 0.0001 compared with WT-S1PR1 or siBiP plus Y143D-S1PR1 by one-way ANOVA with two-tailed paired t test. **(C)** ECs transducing BiP siRNA and S1PR1 mutants as in A were stimulated with 1 µM S1P. Ca^{2+} release (first peak) or SOCE (second peak) was determined as in Fig. 6 G. **(D)** Mean ± SD of increase in Ca^{2+} (n = 8–10 cells/group) from experiments repeated three times. Basal Ca^{2+} (–) analyzed at 20 s; peak increase in Ca^{2+} from ER analyzed at 45 s while peak of SOCE was analyzed at 210 s. **, P < 0.001; ***, P < 0.0001 compared with unstimulated WT-S1PR1 or Y143D-S1PR1; ##, P < 0.001; ###, P < 0.0001 compared with S1P-stimulated WT-S1PR1 by one-way ANOVA with two-tailed paired t test. **(E)** TEER in response to 1 µM S1P from ECs transducing BiP siRNA and S1PR1 mutants as in A. **(F)** Mean ± SD of TEER from experiments repeated three times. Basal TEER was calculated as mean between 10 and 30 min, while S1P-stimulated TEER was the mean between 1 and 1.5 h. ***, P < 0.0001 compared with unstimulated WT-S1PR1 or Y143D-S1PR1; ###, P < 0.0001 compared with unstimulated siBiP plus WT-S1PR1 by one-way ANOVA with two-tailed paired t test. See also Figs. S4, C and D; and S5, A and B. A.U, arbitrary units.

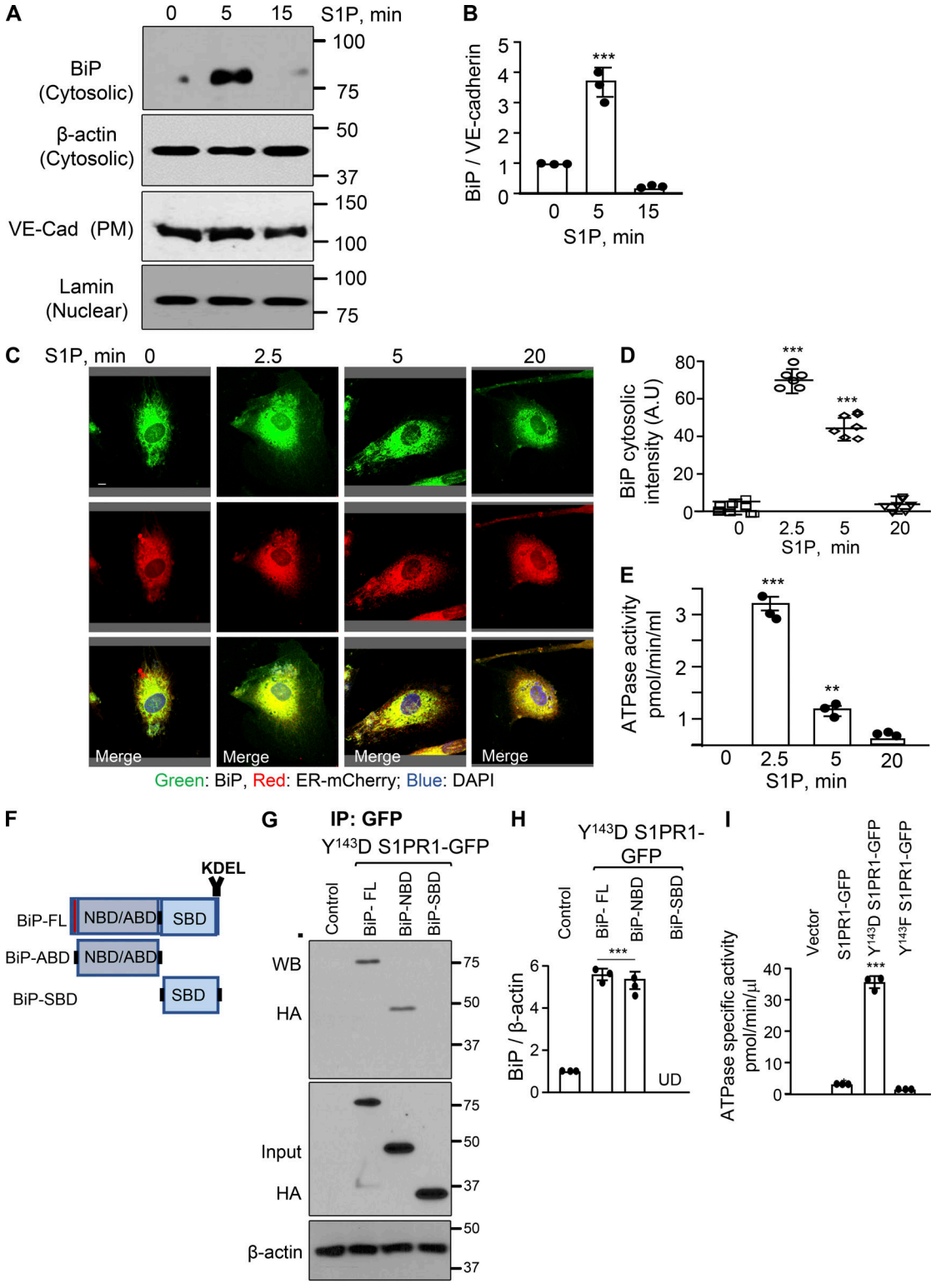

Figure 8. **S1P induces BiP recruitment to the cytosol and activates its ATPase activity, which in turn binds tyrosine-phosphorylated receptor. (A)** Cell fractionation from unstimulated or S1P (1 µM)-stimulated HUVECs after indicated times. **(B)** Mean ± SD of BiP density in cytosolic fraction, using VE-cadherin as the loading control. Fold increase in BiP/VE-cadherin density was calculated against values at time 0 (no S1P addition). ***, P < 0.0001 compared with unstimulated ECs by one-way ANOVA with two-tailed paired *t* test. **(C)** Confocal images showing BiP translocation from ECs transducing ER-mCherry without or with 1 µM S1P stimulation. Cells were stained with anti-BiP antibody and DAPI (to assess nucleus). Images taken at 63× magnification. Scale bar, 5 µm. Gray background indicates the area outside the image. **(D)** Mean ± SD of the BiP expression in the cytosol (4–8 cells/group) from experiments repeated multiple times. ***, P < 0.0001 compared with unstimulated ECs by one-way ANOVA with two-tailed paired *t* test. **(E)** Unstimulated or S1P (1 µM)-stimulated ECs were immunoprecipitated with anti-BiP antibody, and immunocomplexes were used to measure ATPase activity. **, P < 0.001; ***, P < 0.0001 compared with

stimulated ECs at 20 min by one-way ANOVA with two-tailed paired *t* test. **(F)** Physical map of full-length BiP and deletion mutants. **(G)** Pulldown of S1PR1 from HUVECs cotransducing either HA-tagged vector (control), HA-full-length BiP, HA-BiP-ATPase domain, or HA-BiP-SBD domain along with Y^{143}D-S1PR1-GFP. Anti-GFP was used for pulldown. Immunocomplexes were probed with anti-HA antibody to assess BiP expression. **(H)** Mean ± SD BiP interaction with S1PR1. Experiments were repeated at least three times independently. ***, P < 0.0001 compared with vector (control) by one-way ANOVA with two-tailed paired *t* test. **(I)** Mean ± SD of BiP ATPase activity in ECs transducing indicated cDNAs was determined as described in E. *, P < 0.05; ***, P < 0.0001 compared with vector by one-way ANOVA with two-tailed paired *t* test. ABD, ATP-binding domain (ATPase domain); A.U, arbitrary units; Cad, cadherin; FL, full-length; IP, immunoprecipitation; NBD, nucleotide-binding domain; PM, plasma membrane; UD, undetectable; WB, Western blot. **(A and G)** Molecular weight marker in kD.

Y^{143}D-S1PR1 compared with WT-S1PR1. Intriguingly, we show that inhibition of Gi also blocked the ER Ca^{2+} release and that SOCE was induced not only by WT-S1PR1 but also by ER-resident Y^{143}D-S1PR1, indicating that the mutant signaled in a Gi-dependent manner. Consistent with these functional findings, mutant S1PR1 pulled down Gi as well as the nascent S1PR1. Furthermore, Gi inhibition had no effect on disruption of endothelial barrier function induced by the mutant, indicating the involvement of an intermittent mediator compromising EC barrier function in an SOCE-dependent manner. Previous findings that internalized S1PR1 can function in T cells lends credence to our findings and interpretations (Benechet et al., 2016). However, in T cells, internalized S1PR1 regulated signaling independently of Gi (Baeyens et al., 2015). These findings led us to propose that internalized Y^{143}D-S1PR1 mutant interacts with intracellular Gi, consistent with the idea that G proteins localized both at the cell surface and in intracellular compartments can lead to increased Ca^{2+} signaling (Magalhaes et al., 2012).

The present work identified the key role of BiP as a mechanism by which Y^{143}D-S1PR1 mutant gained access to the ER where it led to augmented SOCE and EC barrier disruption. BiP is known to regulate ER stress, operationally defined as impaired calcium homeostasis (Gardner et al., 2013). A few studies also showed that BiP contributes to the regulation of EC barrier function (Leonard et al., 2019). We show that depletion of Rab-GTPases, which sort endocytosed receptors to subcellular compartments (de Renzis et al., 2002; Naslavsky and Caplan, 2018), had no effect on S1PR1 trafficking to the ER. Interestingly, mass spectrometry and pulldown experiments identified BiP, which primarily resides in the ER due to its KDEL motif (Ni et al., 2011), as a novel partner of phosphorylated S1PR1. We also showed that depletion of BiP reversed SOCE and the barrier disruption caused by the Y^{143}D-S1PR1 mutant. Additionally, TNF-α compromised EC barrier function by mediating interaction of Y^{143}-S1PR1 to BiP. Thus, knockdown of BiP prevented EC barrier dysfunction by TNF-α. We infer from these findings that long-lasting phosphorylation of the Y^{143} residue and its coupling with BiP at the ER disrupts the barrier by augmenting SOCE. Our findings that ER-resident S1PR1 is functional has precedence. Studies showed that melanocortin 4 receptor, a GPCR expressed in neurons of the hypothalamus central to the control of appetite, localizes to the ER where it avoids desensitization and thereby potently signals in response to α-melanocyte–stimulating hormone stimulation (Granell et al., 2013). Other open questions to be addressed in future studies are the mechanisms by which BiP and ER-resident Y^{143}D-S1PR1 induce SOCE to impair barrier function.

BiP can localize to the cytosol as well as to membrane fractions, depending on cellular context (Sun et al., 2006). In addition to its ER-retaining KDEL motif, BiP contains an N-terminal nucleotide/ATPase domain and SBD (Adams et al., 2019). Studies also show that an increase in BiP ATPase activity is required for its interaction with cellular proteins (Kopp et al., 2019). Findings from the current studies showed that S1P induced BiP translocation to the cytosol. We also showed that S1PR1 interacted with BiP through the ATPase domain in association with an increase in BiP ATPase activity. While the mechanism by which S1P induces BiP translocation to the cytosol and increases its ATPase activity remains unclear, we conclude that BiP binds endocytosed S1PR1 or the Y^{143}D-S1PR1 mutant in the cytosol to promote their transport to the ER.

Another unanswered question our study raised is how ER-resident Y^{143}D-S1PR1 responds to S1P. While we show that ER-resident S1PR1 responds to S1P in both ECs and HEK cells overexpressing Y^{143}D-S1PR1, the topography of ER-localized S1PR1 is unclear. S1P is a polar lipid and cannot easily permeate the inside cell (Hannun and Obeid, 2008; Saba and Hla, 2004). Extracellular S1P is hydrolyzed by lipid phosphate phosphatases to sphingosine, which is taken up by the cell and converted to S1P by SPHK1 or SPHK2. Extracellular S1P also stimulates sphingosine kinase (SPHK) activity, leading to generation of intracellular S1P (Zhao et al., 2007). Both SPHK1 and SPHK2 are shown to be localized in intracellular organelles, including the ER (Maceyka et al., 2012). SPNS2, the lipid transporter, exports SPHK-derived S1P from inside of cells to outside for S1P to ligate S1PR1 or other S1PRs on the outer leaflet of the plasma membrane (Spiegel et al., 2019). Thus, based on the crystal structure of S1PR1, which revealed that S1P binds to its lateral surface (Hanson et al., 2012), we postulate that extracellular S1P or TNF-α stimulates intracellular S1P generation via SPHK1/SPHK2, which can stimulate ER-localized S1PR1, leading to induction of SOCE and barrier dysfunction. This is likely to be the case because depletion of BiP restored the Y^{143}D-S1PR1 mutant on the EC surface, inhibited SOCE, and rescued EC barrier function.

The conserved E/DRY motif in GPCRs of the class A family is known to be critically important to the receptor's physiological functions and G protein–binding properties. Mutation of glutamic acid (E) or arginine (R) within this triad induces receptor internalization and dramatically affects its G protein coupling and downstream signaling (Rovati et al., 2007). However, until now, the Y residue within this triad was thought to have a minimal impact on GPCR signaling. Here, we established that phosphorylation of Y^{143} within this triad plays a key role in regulating S1PR1 function. Another unique finding made in this study is that Y^{143}D-S1PR1 internalized WT-S1PR1 and disrupted barrier function. Therefore, we conclude from these findings that Y^{143}D-S1PR1 functions as a dominant negative subverting

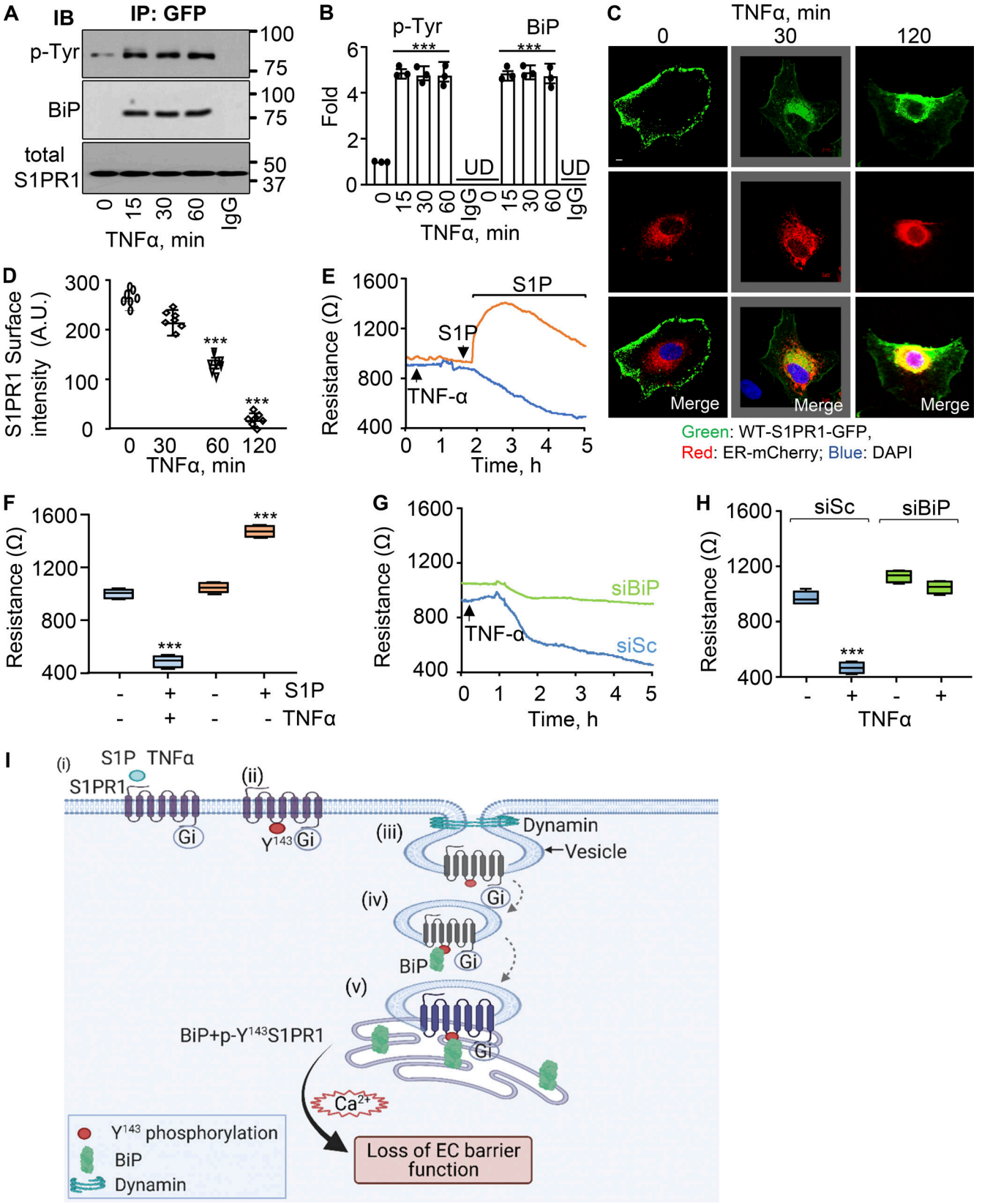

Figure 9. **TNF-α disrupts barrier function by mediating S1PR1 phosphorylation at Y^{143}. (A)** Pulldown of WT-S1PR1 from ECs without or with 50 ng/ml TNF-α stimulation at indicated times using anti-GFP antibody. Immunocomplexes were Western blotted with anti-phosphotyrosine (PY20/PY99) and anti-BiP antibodies. Western blotting with anti-S1PR1 antibody was used for total S1PR1 expression. **(B)** Mean ± SD of tyrosine phosphorylation. *n* = 3 experiments performed independently. ***, P < 0.0001 compared with unstimulated cells by one-way ANOVA with two-tailed paired *t* test. **(C)** Time-lapse images from ECs

cotransducing indicated cDNAs following stimulation with TNF-α. Image taken at 63× magnification. Scale bar, 5 µm. Gray background indicates the area outside the image. **(D)** Mean ± SD of the surface expression of S1PR1 (5–7 cells/group) from experiments performed multiple times. ***, P < 0.0001 compared with unstimulated cells by one-way ANOVA with two-tailed paired *t* test. **(E)** TEER was recorded in control ECs after stimulation with vehicle or 50 ng/ml TNF-α. After 2 h, 1 µM S1P was added to assess the effect of TNF-α–mediated internalization of S1PR1 (observed in C and D) on barrier function. **(F)** Mean ± SD of the TEER from experiments performed three times. Basal TEER was calculated as mean between 10 and 20 min and between 3 and 4 h after S1P addition. ***, P < 0.0001 compared with unstimulated cells by one-way ANOVA with two-tailed paired *t* test. **(G)** TEER was recorded in BiP-depleted ECs after addition of a single dose of 50 ng/ml TNF-α. **(H)** Mean ± SD of the TEER from experiments performed three times. Basal TEER (–) in control and BiP-depleted ECs was analyzed as mean between 10 and 20 min. TNF-α (+)–induced loss of EC barrier function in control or BiP-depleted ECs was calculated as mean between 3.5 and 4 h. ***, P < 0.0001 compared with unstimulated siSc by one-way ANOVA with two-tailed paired *t* test. **(I)** Model shows the effect of tyrosine phosphorylation (Y^{143}) of S1PR1 within ERY motif in regulating receptor function. S1P or TNF-α binds S1PR1 (i) and phosphorylates S1PR1 at Y^{143} (ii; represented as red circle). Dynamin pinches off the phosphorylated S1PR1 (iii). S1P also induces BiP ATPase activity and its translocation to cytosol (not shown). Phosphorylated S1PR1 (Y^{143}D-S1PR1) interacts with BiP in the cytosol (iv). BiP imports the receptor to the ER (v). WT-S1PR1 induces Ca^{2+} signaling and returns to the cell surface after dephosphorylation (not shown). BiP traps the Y^{143}D-S1PR1 mutant at the ER where it augments SOCE and induces barrier-disruptive signaling in a Gi-dependent manner. See also Fig. S5, C and D. A.U., arbitrary units; IB, immunoblot; IP, immunoprecipitation; p-Tyr, phosphorylated tyrosine; UD, undetectable. **(A)** Molecular weight marker in kD.

the canonical barrier maintaining function of S1PR1 in ECs. Indeed, findings from the current study show that during inflammation, sustained S1PR1 phosphorylation at Y^{143} through its interaction with BiP induces counterproductive S1PR1 signaling to disrupt barrier function. Whether Y^{143}D mutation in S1PR1 is the cause of vascular leak in susceptible lung injury patients remains to be investigated. We have thus identified phosphorylation of the S1PR1-ERY motif as a new and targetable mechanism of endothelial barrier breakdown common to lung and other organs.

In conclusion, our studies address the fundamental mechanisms regulating the fate of tyrosine phosphorylated S1PR1, as shown in Fig. 9 I, because it is evident that Y^{143}D-S1PR1, in contrast to the native receptor, plays a critical role in triggering barrier-disruptive rather than barrier-enhancing signaling, and that has great potential as a therapeutic target. The widespread expression of BiP, along with the conserved E/DRY motif in class A GPCRs, suggests that the regulatory functions of the Y residue within the triad extend well beyond the physiological effects of S1PR1 exemplified in the current study.

Materials and methods

Materials

S1PR1 antibody was purchased either from Alomone Labs (cat. #ASR-011) or Santa Cruz Biotechnology (sc-48356). Dynamin I/II (cat. #2342), Rab5 (cat. #3547), Rab7 (cat. #9367), Lamin A (cat. #86846), HA-tag (cat. #3724), and BiP[C50B12] (cat. #3177) antibodies were procured from Cell Signaling Technologies. Giα-1 and VE-cadherin antibodies were purchased from Santa Cruz Biotechnology (sc-13533), while β-actin was from Invitrogen (cat. #MA5-15739). Phosphotyrosine (PY99/PY20, sc-7020 and sc-508) and GFP (sc-9996) antibodies and Protein A/G PLUS-Agarose (sc-2003) were from Santa Cruz Biotechnology. Pierce Streptavidin Agarose beads (cat. #20349), Pierce Biotin (cat. #29129), Prolong Gold Antifade (cat. #P10144), SuperSignal West Pico Chemiluminescent Substrate (cat. #34580), and Halt Protease and Phosphatase Inhibitor Cocktail (100×; cat. #78446) were from Thermo Fisher Scientific. S1P, D-erythro (cat. #BML-SL140-0001) was from Enzo Life Sciences. Dynasore hydrate (cat. #D7693-5MG) and PTX (cat. #P7208) were from MilliporeSigma. VECTASHIELD antifade mounting medium with DAPI (cat. #H-1200) was from Vector Laboratories. Recombinant human TNF-α (cat. #300-01A) was from PeproTech. Fura-2 AM, a Ca^{2+}-selective fluorescence indicator (ab120873) was from Abcam.

Plasmids

All phosphorylation-specific GFP-tagged S1PR1 constructs were created as previously described (Chavez et al., 2015). ER-mCherry was provided by Y. Komarova. WT-dynamin2-mCherry and dominant-negative (K44A) dynamin-mCherry have been previously published (Shajahan et al., 2004). BiP-mCherry-KDEL (cat. #62233) was from Addgene. S1PR1-Dendra2 construct was generated by a PCR-based strategy and subcloning S1PR1-GFP and Dendra2 (Daneshjou et al., 2015). The primer sequences for subcloning S1PR1-GFP and Dendra2 are as follows: forward primer, 5′-TCGAATGGCACGAAGGAGGCGGACCGGTCG CCACCATGAACACCCCGGGAATTAACCTGA-3′, reverse primer, 5′-ATGGCTGATTATGATCTAGAGTCGCGGCCGCTTTACCACACC TGGCTGGGCAGGGGGCTG-3′. All cDNA sequences were confirmed against their GenBank accession numbers. These cDNAs were transfected in HUVECs or HEK293 cells using Amaxa Nucleofector (Lonza) or FuGENE HD (Roche).

Cell culture

HUVECs obtained from Lonza (cat. #C2519) were cultured by the same procedure as previously described (Yazbeck et al., 2017). Briefly, cells were plated in a T-75 flask (BD Falcon) coated with 0.1% gelatin and cultured in EBM-2 media (Lonza) supplemented with growth factors and 10% FBS (Thermo Fisher Scientific). Cells were cultured in a 37°C humidified incubator in the presence of 5% CO_2 and 95% O_2 until they formed a monolayer and achieved the desired confluence. HUVECs between passages 5 and 6 were used for these studies. The HEK293 cell line (American Type Culture Collection) was cultured in DMEM (Gibco) supplemented with 10% FBS (Thermo Fisher Scientific) and 5% penicillin/streptomycin (Thermo Fisher Scientific). HEK293 cells were transfected with indicated cDNAs using FuGENE HD (Roche).

Transfections

All siRNA sequences as well as ON-TARGETplus Non-targeting Control Pool (D-001810-10) sequences were purchased from

Dharmacon. Dynamin-2 or BiP (GRP78) or Rab5 and 7 were depleted using the following siRNA sequences: dynamin-2 antisense sequence, 5′-GACAUGAUCCUGCAGUUCAUU-3′; BiP siRNA, 5′-...CGAGUGACAGCUGAAGACAAGGGUA-3′; Rab5 siRNA, 5′-GGAAGAGGAGUAGACCUUA-3′; and Rab7 siRNA, 5′-GCUGCG UUCUGGUAUUUGA-3′. Cells were transfected with indicated siRNAs using either a Santa Cruz Biotechnology transfection reagent or an Amaxa Nucleofector (Lonza) electroporation system as previously described (Chavez et al., 2015; Yazbeck et al., 2017).

ECs were cotransfected with WT-S1PR1-GFP, Y^{143}D-S1PR1-GFP, or Y^{143}F-S1PR1-GFP cDNAs along with GTPase-defective dynamin (K44A) or control vector using Amaxa reagent. 24 h after transfection, cells were serum starved and then processed either for imaging or for biochemical analysis (Chavez et al., 2015). The transfection efficiency for GFP was 90%, while efficiency for S1PR1, dynamin, and other cDNAs, which include BiP, ER-mCherry, HA-tagged S1PR1 cDNAs and S1PR1-Dendra2, ranged between 40% and 60%.

Immunoprecipitation and Western blotting

For immunoprecipitation analysis, post-S1P or -TNF-α stimulation serum-starved ECs were stimulated with 1 µM S1P or 50 ng/ml TNF-α. Cells were washed with ice-cold PBS and immediately lysed in modified radioimmunoprecipitation assay (RIPA) buffer (50 mM Tris, pH 7.4, 150 mM NaCl, 10% lubrol, 1% NP-40, 25 mM $MgCl_2$, 1 mM PMSF, 25 mM NaF, 1 mM $NaVO_4$, 1% protease inhibitor cocktail, and 1% phosphatase inhibitor cocktail). Lysates were incubated with anti-GFP (1:200) or anti-S1PR1 (1:100) antibodies overnight followed by the addition of agarose beads to pull down the immunocomplexes (Chavez et al., 2015). Proteins were separated by SDS-PAGE and immunoblotted using indicated antibodies. Dilution for each primary antibody used in the study were as follows: S1PR1 (1:500), dynamin I/II (1:1,000), BiP (1:1,000), VE-cadherin (1:500), Lamin A (1:1,000), Rab5 (1:1,000), Rab7 (1:1,000), HA-tag (1:1,000), GFP (1:500), phosphotyrosine (PY99/PY20, 1:250), Giα (1:500), and β-actin (1:1,000). Membranes were then incubated with respective secondary antibodies anti-mouse or anti-rabbit (1:10,000) for 2 h, following which the bands were visualized using imager or autoradiographic films and chemiluminescent Western blotting detection substrate.

Biotinylation assay

HUVECs were washed with ice-cold PBS, after which cells were labeled with 0.5 mg/ml sulfo-NHS-SS Biotin in Ca^{2+}/Mg^{2+} containing PBS for 30 min at 4°C. The reaction was then quenched using 100 mM glycine for 20 min, after which cells were harvested in RIPA buffer containing 10% lubrol. Equal amounts of protein were incubated with streptavidin agarose resin beads at 4°C overnight followed by three times centrifugation at 2,400 *g* and rinsing using RIPA buffer at 4°C. Proteins were then eluted using 4× Laemmli buffer and Western blotted as described previously (Chavez et al., 2015).

Confocal and TIRF imaging

HUVECs seeded on 35-mm Nunc glass-bottom dishes (Thermo Fisher Scientific) were transfected with indicated cDNA or siRNA. 24 or 48 h after transfection, cells were serum starved in basal media supplemented with 0.1% FBS for 1–2 h followed by quick rinse with PBS. Cells were then stimulated with indicated agonists and fixed at indicated times with 2% paraformaldehyde and mounted as described previously (Chavez et al., 2015). In some studies, cells were permeabilized after fixation and immunofluorescently stained with anti-BiP, anti-Rab5, or anti-Rab7 antibodies followed by incubation with appropriate fluorescently conjugated secondary antibodies. Confocal images were acquired using an LSM 880 inverted laser scanning system (Carl Zeiss) equipped with Plan-Apochromat 63×/1.4 NA oil immersion objective, argon (λ = 458, 488, 514 nm) and diode-pumped solid-state (λ = 561 nm) lasers, two photomultiplier tubes, and gallium arsenide phosphide detector.

Time-lapse images of S1PR1-Dendra2 were acquired using an LSM 710 Meta inverted laser scanning system (Carl Zeiss) equipped with 63×/1.20 NA and 1.46 NA water and oil immersion objectives, diode 405-30 (λ = 405 nm), argon (λ = 458, 488, 514 nm), DPSS 561-10 (λ = 561 nm), and HeNe (λ = 633 nm) lasers. To determine the effect of S1P on the receptor trafficking, Dendra2 was photoconverted with 405-nm laser at 8–12% power for 10 s at a selected region at the plasma membrane, and dual-channel images were simultaneously acquired using a 63×/1.20 NA objective every 30 s at λ = 488 nm and λ = 561 nm excitations for green and red states of Dendra2, respectively.

TIRF microscopy was performed using a motorized laser TIRF imaging system (Carl Zeiss) equipped with an ORCA-Flash4.0 V3 Digital CMOS camera (Hamamatsu), and an α Plan-Apochromat 100×/1.46 NA objective (Carl Zeiss). For detection of cell surface expression of the receptor, GFP-tagged WT and mutant S1PR1 along with mCherry-tagged stargazin (cell surface marker) were imaged at λ = 488 nm and λ = 561 nm excitation for GFP and mCherry, respectively. Images from green and red channels (excitation 488 nm and 561 nm) were obtained by fast switching the excitation lasers using AxioVision software (Carl Zeiss).

Image processing and analysis

All 16-bit images were analyzed with Fiji image-processing software (ImageJ2; National Institutes of Health). For analysis of cell surface expression of S1PR1, multiple regions of interest of the same size were drawn on the plasma membrane, and pixel intensity was calculated. Intensity obtained from multiple regions of interest from the same cell was average (Schindelin et al., 2012).

The surface expression of S1PR1 and its mutants on TIRF images were determined as the average intensity of the plasma membrane after the digital subtraction of the background.

Colocalization between GFP-S1PR1 or its mutants (Y^{143}D-S1PR1 and Y^{143}F-S1PR1) and mCherry-tagged BiP, ER, or GTPase-defective dynamin (K44A) mutant was quantified using the Colocalization Threshold plugin of ImageJ.

S1PR1 trafficking was assessed by measuring fluorescent intensity of Dendra2 in red state over time after Dendra2 photoconversion at the plasma membrane. Changes in cell surface localization of S1PR1 due to receptor internalization were determined as a loss of red fluorescent signal within the photoconversion region over time after subtraction of the average

background fluorescence values. The levels of internalized S1PR1 were determined as increase of red fluorescent signal over time inside the cell over the cell area after subtracting the background.

Calcium imaging

Increase in $[Ca^{2+}]_i$ was determined using Ca^{2+}-sensitive fluorescent dye Fura-2 AM as described earlier (Sundivakkam et al., 2012; Yazbeck et al., 2017). Briefly, HUVECs or HEK293 cells transfected with indicated cDNAs or siRNAs for 24–48 h were loaded with Fura-2 AM dye for 15–20 min. Cells were rinsed with Ca^{2+}-free HBSS buffer. In this study, only GFP-expressing cells were chosen for Ca^{2+} imaging. Ca^{2+} entry was determined by the readdition of 1.5 mM Ca^{2+} in ECs bathed in Ca^{2+}-free solution and S1P.

Mass spectrometry analysis

HUVECs were transfected with WT-S1PR1, Y^{143}D-S1PR1, or Y^{143}F-S1PR1 for 24 h. HUVECs expressing WT-S1PR1-GFP were serum starved for 2 h and stimulated with S1P for 0, 5, and 15 min. These time points were chosen based on S1PR1 phosphorylation-dephosphorylation following S1P stimulation (Chavez et al., 2015). ECs expressing Y^{143}D-S1PR1 or Y^{143}F-S1PR1 for 24 h were also serum starved for 2 h and were left unstimulated. Cells were lysed with 10% lubrol containing RIPA buffer (as above for immunoprecipitation studies), and equal amounts of lysates were immunoprecipitated with anti-GFP antibody overnight at 4°C, after which complexes were pull down with protein A/G agarose beads. After confirming S1PR1 expression using Western blot, immunocomplexes were separated on 7.5% gel for up to 2 cm, following which the gel was stained using Coomassie brilliant blue and washed using distilled water. Gel lanes were cut and then analyzed at the Harvard mass spectrometry facility. The datasets of spectral counts and intensity scores were calculated and further quantified using Ingenuity Pathway Analysis. Nonunique peptides were excluded from the mass spectrometry data. Only unique candidates in the context of S1PR1 complexes were shown with greater intensities and arbitrarily chosen $\log_{10}$ mean peptide scores. These proteins were evaluated for known interactions with other interaction databases. We focused on BiP (HSPA5) as (1) it is an ER-localized protein and (2) it binds S1PR1 with the highest intensity peptide score among the interactome in the phosphorylated state of S1PR1. Scatter plot of mean intensity versus spectral position was generated using ggplot2. Later, this interaction was further validated using immunoprecipitation studies.

TEER measurements

HUVECs seeded on eight-well gold-plated electrodes (Applied Biosciences) were transfected with either indicated siRNAs (48 h) or cDNAs (24 h). At indicated times after transfection, cells were serum starved for 1–2 h, and basal TEER was recorded. Cells were then stimulated with either 1 µM S1P (Chavez et al., 2015; Tauseef et al., 2008), 50 ng/ml TNF-α, or 50 µM PTX. Note that all the studies were performed in confluent monolayer, which was confirmed by forming a cell monolayer showing a resistance of ∼1,000 Ω.

ATPase activity measurements

ATPase activity was determined using a Malachite Green Phosphate Assay Kit (BioVision) according to the manufacturer's instructions. Reaction mixtures were prepared in triplicate in a final volume of 200 µl, using 10 µg of protein dissolved in 30 mM Hepes-KOH (pH 7.8), 150 mM NaCl, 20 µM ATP, and 2 mM $MgCl_2$. Samples were incubated for 60 min at 37°C, after which the concentration of phosphate was measured at 620–650 nm using a SpectraMax 340PC Microplate Reader (Bio-Rad). The resulting data were analyzed and kinetic parameters calculated using the Michaelis–Menten equation with GraphPad Prism 5 software (GraphPad Software).

Subcellular localization of BiP

Serum-deprived ECs were stimulated with S1P for indicated times, after which subcellular fractionation was performed using Cell Fractionation Kit (cat. #78840; Thermo Scientific Scientific) and the manufacturer's protocol. Different subcellular protein fractions were run on SDS-PAGE and probed for respective markers.

Quantification and statistics

The statistical analysis was performed using GraphPad Prism 7.0 software. The specific statistical methods used for individual experiments are mentioned in the figure legends with their significance values. Paired *t* tests were performed for experiments containing two groups, while one-way ANOVA was performed in experiments containing multiple groups. Data distribution was assumed to be normal, but this was not formally tested. The following P values were used in the study for the significance: *, $P < 0.05$ was considered significant; **, $P < 0.001$ was considered highly significant; and ***, $P < 0.0001$ was considered very highly significant.

Online supplemental material

Fig. S1 shows S1PR1 localization. Fig. S2 shows S1PR1 internalization independent of Rab-GTPases. Fig. S3 shows mass spectrometric analysis of S1PR1 binding partners. Fig. S4 shows the effect of inhibition of Gi on cytosolic calcium and barrier function in response to S1P. Fig. S5 shows that TNF-α fails to phosphorylate Y^{143}F-S1PR1.

Acknowledgments

We thank Dr. Mark Rasenick (Department of Physiology and Biophysics, University of Illinois at Chicago) for discussion. We thank Dr. Peter Toth (Imaging Core, Research Resources Center, University of Illinois at Chicago) for help in imaging.

This work was supported by National Institutes of Health grants HL84153, HL060678, and HL137169.

The authors declare no competing financial interests.

Author contributions: M. Anwar, Y. Komarova, and D. Mehta conceived the project. M. Anwar and D. Mehta designed the experiments. M. Anwar, M.R. Amin and V.A. Balaji Ragunathrao

performed experiments and analyzed the data. J. Matsche and A. Karginov generated Dendra2-S1PR1 cDNA. R.D. Minshall, G.C.H. Mo, and Y. Komarova helped with imaging and preparation of figures and commented on the manuscript. M. Anwar and D. Mehta interpreted data and wrote the manuscript.

Submitted: 4 June 2020
Revised: 2 November 2020
Accepted: 15 June 2021

References

Adams, B.M., M.E. Oster, and D.N. Hebert. 2019. Protein quality control in the endoplasmic reticulum. *Protein J.* 38:317–329. https://doi.org/10.1007/s10930-019-09831-w

Anwar, M., and D. Mehta. 2020. Post-translational modifications of S1PR1 and endothelial barrier regulation. *Biochim. Biophys. Acta Mol. Cell Biol. Lipids.* 1865:158760. https://doi.org/10.1016/j.bbalip.2020.158760

Baeyens, A., V. Fang, C. Chen, and S.R. Schwab. 2015. Exit strategies: S1P signaling and T cell migration. *Trends Immunol.* 36:778–787. https://doi.org/10.1016/j.it.2015.10.005

Balaji Ragunathrao, V.A., M. Anwar, M.Z. Akhter, A. Chavez, Y. Mao, V. Natarajan, S. Lakshmikanthan, M. Chrzanowska-Wodnicka, A.Z. Dudek, L. Claesson-Welsh, et al. 2019. Sphingosine-1-phosphate receptor 1 activity promotes tumor growth by amplifying VEGF-VEGFR2 angiogenic signaling. *Cell Rep.* 29:3472–3487.e4. https://doi.org/10.1016/j.celrep.2019.11.036

Benechet, A.P., M. Menon, D. Xu, T. Samji, L. Maher, T.T. Murooka, T.R. Mempel, B.S. Sheridan, F.M. Lemoine, and K.M. Khanna. 2016. T cell-intrinsic S1PR1 regulates endogenous effector T-cell egress dynamics from lymph nodes during infection. *Proc. Natl. Acad. Sci. USA.* 113:2182–2187. https://doi.org/10.1073/pnas.1516485113

Cahalan, S.M., P.J. Gonzalez-Cabrera, G. Sarkisyan, N. Nguyen, M.T. Schaeffer, L. Huang, A. Yeager, B. Clemons, F. Scott, and H. Rosen. 2011. Actions of a picomolar short-acting $S1P_1$ agonist in $S1P_1$-eGFP knock-in mice. *Nat. Chem. Biol.* 7:254–256. https://doi.org/10.1038/nchembio.547

Cannavo, A., G. Rengo, D. Liccardo, G. Pagano, C. Zincarelli, M.C. De Angelis, R. Puglia, E. Di Pietro, J.E. Rabinowitz, M.V. Barone, et al. 2013. β1-Adrenergic receptor and sphingosine-1-phosphate receptor 1 (S1PR1) reciprocal downregulation influences cardiac hypertrophic response and progression to heart failure: protective role of S1PR1 cardiac gene therapy. *Circulation.* 128:1612–1622. https://doi.org/10.1161/CIRCULATIONAHA.113.002659

Carrara, M., F. Prischi, P.R. Nowak, M.C. Kopp, and M.M. Ali. 2015. Non-canonical binding of BiP ATPase domain to Ire1 and Perk is dissociated by unfolded protein CH1 to initiate ER stress signaling. *eLife.* 4:e03522. https://doi.org/10.7554/eLife.03522

Cartier, A., and T. Hla. 2019. Sphingosine 1-phosphate: Lipid signaling in pathology and therapy. *Science.* 366:eaar5551. https://doi.org/10.1126/science.aar5551

Chavez, A., T.T. Schmidt, P. Yazbeck, C. Rajput, B. Desai, S. Sukriti, K. Giantsos-Adams, N. Knezevic, A.B. Malik, and D. Mehta. 2015. S1PR1 Tyr143 phosphorylation downregulates endothelial cell surface S1PR1 expression and responsiveness. *J. Cell Sci.* 128:878–887. https://doi.org/10.1242/jcs.154476

Chichger, H., J. Braza, H. Duong, G. Boni, and E.O. Harrington. 2016. Select Rab GTPases regulate the pulmonary endothelium via endosomal trafficking of vascular endothelial-cadherin. *Am. J. Respir. Cell Mol. Biol.* 54:769–781. https://doi.org/10.1165/rcmb.2015-0286OC

Chudakov, D.M., S. Lukyanov, and K.A. Lukyanov. 2007. Tracking intracellular protein movements using photoswitchable fluorescent proteins PS-CFP2 and Dendra2. *Nat. Protoc.* 2:2024–2032. https://doi.org/10.1038/nprot.2007.291

Cyster, J.G., and S.R. Schwab. 2012. Sphingosine-1-phosphate and lymphocyte egress from lymphoid organs. *Annu. Rev. Immunol.* 30:69–94. https://doi.org/10.1146/annurev-immunol-020711-075011

Damke, H., D.D. Binns, H. Ueda, S.L. Schmid, and T. Baba. 2001. Dynamin GTPase domain mutants block endocytic vesicle formation at morphologically distinct stages. *Mol. Biol. Cell.* 12:2578–2589. https://doi.org/10.1091/mbc.12.9.2578

Daneshjou, N., N. Sieracki, G.P. van Nieuw Amerongen, D.E. Conway, M.A. Schwartz, Y.A. Komarova, and A.B. Malik. 2015. Rac1 functions as a reversible tension modulator to stabilize VE-cadherin trans-interaction. *J. Cell Biol.* 208:23–32. https://doi.org/10.1083/jcb.201409108

de Renzis, S., B. Sönnichsen, and M. Zerial. 2002. Divalent Rab effectors regulate the sub-compartmental organization and sorting of early endosomes. *Nat. Cell Biol.* 4:124–133. https://doi.org/10.1038/ncb744

DeLalio, L.J., M. Billaud, C.A. Ruddiman, S.R. Johnstone, J.T. Butcher, A.G. Wolpe, X. Jin, T.C.S. Keller IV, A.S. Keller, T. Rivière, et al. 2019. Constitutive SRC-mediated phosphorylation of pannexin 1 at tyrosine 198 occurs at the plasma membrane. *J. Biol. Chem.* 294:6940–6956. https://doi.org/10.1074/jbc.RA118.006982

Dickens, J.A., A. Ordóñez, J.E. Chambers, A.J. Beckett, V. Patel, E. Malzer, C.S. Dominicus, J. Bradley, A.A. Peden, I.A. Prior, et al. 2016. The endoplasmic reticulum remains functionally connected by vesicular transport after its fragmentation in cells expressing Z-α1-antitrypsin. *FASEB J.* 30:4083–4097. https://doi.org/10.1096/fj.201600430R

Doronzo, G., E. Astanina, D. Corà, G. Chiabotto, V. Comunanza, A. Noghero, F. Neri, A. Puliafito, L. Primo, C. Spampanato, et al. 2019. TFEB controls vascular development by regulating the proliferation of endothelial cells. *EMBO J.* 38:201798250. https://doi.org/10.15252/embj.201798250

Drake, M.T., S.K. Shenoy, and R.J. Lefkowitz. 2006. Trafficking of G protein-coupled receptors. *Circ. Res.* 99:570–582. https://doi.org/10.1161/01.RES.0000242563.47507.ce

Dudek, S.M., J.R. Jacobson, E.T. Chiang, K.G. Birukov, P. Wang, X. Zhan, and J.G. Garcia. 2004. Pulmonary endothelial cell barrier enhancement by sphingosine 1-phosphate: Roles for cortactin and myosin light chain kinase. *J. Biol. Chem.* 279:24692–24700. https://doi.org/10.1074/jbc.M313969200

Engelbrecht, E., M.V. Levesque, L. He, M. Vanlandewijck, A. Nitzsche, H. Niazi, A. Kuo, S.A. Singh, M. Aikawa, K. Holton, et al. 2020. Sphingosine 1-phosphate-regulated transcriptomes in heterogenous arterial and lymphatic endothelium of the aorta. *eLife.* 9:e52690. https://doi.org/10.7554/eLife.52690

Ferguson, S.M., and P. De Camilli. 2012. Dynamin, a membrane-remodelling GTPase. *Nat. Rev. Mol. Cell Biol.* 13:75–88. https://doi.org/10.1038/nrm3266

Gardner, B.M., D. Pincus, K. Gotthardt, C.M. Gallagher, and P. Walter. 2013. Endoplasmic reticulum stress sensing in the unfolded protein response. *Cold Spring Harb. Perspect. Biol.* 5:a013169. https://doi.org/10.1101/cshperspect.a013169

Gorvel, J.P., P. Chavrier, M. Zerial, and J. Gruenberg. 1991. rab5 controls early endosome fusion in vitro. *Cell.* 64:915–925. https://doi.org/10.1016/0092-8674(91)90316-Q

Granell, S., B.M. Molden, and G. Baldini. 2013. Exposure of MC4R to agonist in the endoplasmic reticulum stabilizes an active conformation of the receptor that does not desensitize. *Proc. Natl. Acad. Sci. USA.* 110:E4733–E4742. https://doi.org/10.1073/pnas.1219808110

Gunther, E.C., C.S. von Bartheld, L.J. Goodman, J.E. Johnson, and M. Bothwell. 2000. The G-protein inhibitor, pertussis toxin, inhibits the secretion of brain-derived neurotrophic factor. *Neuroscience.* 100:569–579. https://doi.org/10.1016/S0306-4522(00)00309-2

Haj, F.G., P.J. Verveer, A. Squire, B.G. Neel, and P.I. Bastiaens. 2002. Imaging sites of receptor dephosphorylation by PTP1B on the surface of the endoplasmic reticulum. *Science.* 295:1708–1711. https://doi.org/10.1126/science.1067566

Hannun, Y.A., and L.M. Obeid. 2008. Principles of bioactive lipid signalling: Lessons from sphingolipids. *Nat. Rev. Mol. Cell Biol.* 9:139–150. https://doi.org/10.1038/nrm2329

Hanson, M.A., C.B. Roth, E. Jo, M.T. Griffith, F.L. Scott, G. Reinhart, H. Desale, B. Clemons, S.M. Cahalan, S.C. Schuerer, et al. 2012. Crystal structure of a lipid G protein-coupled receptor. *Science.* 335:851–855. https://doi.org/10.1126/science.1215904

Hutagalung, A.H., and P.J. Novick. 2011. Role of Rab GTPases in membrane traffic and cell physiology. *Physiol. Rev.* 91:119–149. https://doi.org/10.1152/physrev.00059.2009

Inamura, M., M. Itakura, H. Okamoto, S. Hoka, A. Mizoguchi, Y. Fukazawa, R. Shigemoto, S. Yamamori, and M. Takahashi. 2006. Differential localization and regulation of stargazin-like protein, gamma-8 and stargazin in the plasma membrane of hippocampal and cortical neurons. *Neurosci. Res.* 55:45–53. https://doi.org/10.1016/j.neures.2006.01.004

Jambusaria, A., Z. Hong, L. Zhang, S. Srivastava, A. Jana, P.T. Toth, Y. Dai, A.B. Malik, and J. Rehman. 2020. Endothelial heterogeneity across distinct vascular beds during homeostasis and inflammation. *eLife.* 9:e51413. https://doi.org/10.7554/eLife.51413

Komarova, Y.A., K. Kruse, D. Mehta, and A.B. Malik. 2017. Protein Interactions at endothelial junctions and signaling mechanisms regulating

endothelial permeability. *Circ. Res.* 120:179–206. https://doi.org/10.1161/CIRCRESAHA.116.306534

Kopp, M.C., N. Larburu, V. Durairaj, C.J. Adams, and M.M.U. Ali. 2019. UPR proteins IRE1 and PERK switch BiP from chaperone to ER stress sensor. *Nat. Struct. Mol. Biol.* 26:1053–1062. https://doi.org/10.1038/s41594-019-0324-9

Leonard, A., V. Grose, A.W. Paton, J.C. Paton, D.I. Yule, A. Rahman, and F. Fazal. 2019. Selective Inactivation of Intracellular BiP/GRP78 attenuates endothelial inflammation and permeability in acute lung injury. *Sci. Rep.* 9:2096. https://doi.org/10.1038/s41598-018-38312-w

Li, Q., B. Chen, C. Zeng, A. Fan, Y. Yuan, X. Guo, X. Huang, and Q. Huang. 2015. Differential activation of receptors and signal pathways upon stimulation by different doses of sphingosine-1-phosphate in endothelial cells. *Exp. Physiol.* 100:95–107. https://doi.org/10.1113/expphysiol.2014.082149

Maceyka, M., K.B. Harikumar, S. Milstien, and S. Spiegel. 2012. Sphingosine-1-phosphate signaling and its role in disease. *Trends Cell Biol.* 22:50–60. https://doi.org/10.1016/j.tcb.2011.09.003

Macia, E., M. Ehrlich, R. Massol, E. Boucrot, C. Brunner, and T. Kirchhausen. 2006. Dynasore, a cell-permeable inhibitor of dynamin. *Dev. Cell.* 10: 839–850. https://doi.org/10.1016/j.devcel.2006.04.002

Magalhaes, A.C., H. Dunn, and S.S. Ferguson. 2012. Regulation of GPCR activity, trafficking and localization by GPCR-interacting proteins. *Br. J. Pharmacol.* 165:1717–1736. https://doi.org/10.1111/j.1476-5381.2011.01552.x

Matloubian, M., C.G. Lo, G. Cinamon, M.J. Lesneski, Y. Xu, V. Brinkmann, M.L. Allende, R.L. Proia, and J.G. Cyster. 2004. Lymphocyte egress from thymus and peripheral lymphoid organs is dependent on S1P receptor 1. *Nature.* 427:355–360. https://doi.org/10.1038/nature02284

Mehta, D., and A.B. Malik. 2006. Signaling mechanisms regulating endothelial permeability. *Physiol. Rev.* 86:279–367. https://doi.org/10.1152/physrev.00012.2005

Mehta, D., M. Konstantoulaki, G.U. Ahmmed, and A.B. Malik. 2005. Sphingosine 1-phosphate-induced mobilization of intracellular Ca2+ mediates rac activation and adherens junction assembly in endothelial cells. *J. Biol. Chem.* 280:17320–17328. https://doi.org/10.1074/jbc.M411674200

Naslavsky, N., and S. Caplan. 2018. The enigmatic endosome - sorting the ins and outs of endocytic trafficking. *J. Cell Sci.* 131:jcs216499. https://doi.org/10.1242/jcs.216499

Ni, M., Y. Zhang, and A.S. Lee. 2011. Beyond the endoplasmic reticulum: Atypical GRP78 in cell viability, signalling and therapeutic targeting. *Biochem. J.* 434:181–188. https://doi.org/10.1042/BJ20101569

Oo, M.L., S.H. Chang, S. Thangada, M.T. Wu, K. Rezaul, V. Blaho, S.I. Hwang, D.K. Han, and T. Hla. 2011. Engagement of $S1P_1$-degradative mechanisms leads to vascular leak in mice. *J. Clin. Invest.* 121:2290–2300. https://doi.org/10.1172/JCI45403

Proia, R.L., and T. Hla. 2015. Emerging biology of sphingosine-1-phosphate: Its role in pathogenesis and therapy. *J. Clin. Invest.* 125:1379–1387. https://doi.org/10.1172/JCI76369

Ramsay, D., E. Kellett, M. McVey, S. Rees, and G. Milligan. 2002. Homo- and hetero-oligomeric interactions between G-protein-coupled receptors in living cells monitored by two variants of bioluminescence resonance energy transfer (BRET): Hetero-oligomers between receptor subtypes form more efficiently than between less closely related sequences. *Biochem. J.* 365:429–440. https://doi.org/10.1042/bj20020251

Rasmussen, S.G., B.T. DeVree, Y. Zou, A.C. Kruse, K.Y. Chung, T.S. Kobilka, F.S. Thian, P.S. Chae, E. Pardon, D. Calinski, et al. 2011. Crystal structure of the β2 adrenergic receptor-Gs protein complex. *Nature.* 477:549–555. https://doi.org/10.1038/nature10361

Reinhard, N.R., M. Mastop, T. Yin, Y. Wu, E.K. Bosma, T.W.J. Gadella Jr., J. Goedhart, and P.L. Hordijk. 2017. The balance between $G\alpha_i$-Cdc42/Rac and $G\alpha_{12/13}$-RhoA pathways determines endothelial barrier regulation by sphingosine-1-phosphate. *Mol. Biol. Cell.* 28:3371–3382. https://doi.org/10.1091/mbc.e17-03-0136

Rivera, J., R.L. Proia, and A. Olivera. 2008. The alliance of sphingosine-1-phosphate and its receptors in immunity. *Nat. Rev. Immunol.* 8:753–763. https://doi.org/10.1038/nri2400

Rosenbaum, D.M., S.G. Rasmussen, and B.K. Kobilka. 2009. The structure and function of G-protein-coupled receptors. *Nature.* 459:356–363. https://doi.org/10.1038/nature08144

Rovati, G.E., V. Capra, and R.R. Neubig. 2007. The highly conserved DRY motif of class A G protein-coupled receptors: Beyond the ground state. *Mol. Pharmacol.* 71:959–964. https://doi.org/10.1124/mol.106.029470

Saba, J.D., and T. Hla. 2004. Point-counterpoint of sphingosine 1-phosphate metabolism. *Circ. Res.* 94:724–734. https://doi.org/10.1161/01.RES.0000122383.60368.24

Schindelin, J., I. Arganda-Carreras, E. Frise, V. Kaynig, M. Longair, T. Pietzsch, S. Preibisch, C. Rueden, S. Saalfeld, B. Schmid, et al. 2012. Fiji: An open-source platform for biological-image analysis. *Nat. Methods.* 9: 676–682. https://doi.org/10.1038/nmeth.2019

Shajahan, A.N., B.K. Timblin, R. Sandoval, C. Tiruppathi, A.B. Malik, and R.D. Minshall. 2004. Role of Src-induced dynamin-2 phosphorylation in caveolae-mediated endocytosis in endothelial cells. *J. Biol. Chem.* 279: 20392–20400. https://doi.org/10.1074/jbc.M308710200

Spiegel, S., M.A. Maczis, M. Maceyka, and S. Milstien. 2019. New insights into functions of the sphingosine-1-phosphate transporter SPNS2. *J. Lipid Res.* 60:484–489. https://doi.org/10.1194/jlr.S091959

Sun, F.C., S. Wei, C.W. Li, Y.S. Chang, C.C. Chao, and Y.K. Lai. 2006. Localization of GRP78 to mitochondria under the unfolded protein response. *Biochem. J.* 396:31–39. https://doi.org/10.1042/BJ20051916

Sundivakkam, P. C., M. Freichel, V. Singh, J.P. Yuan, S.M. Vogel, V. Flockerzi, A.B. Malik, and C. Tiruppathi. 2012. The Ca^{2+} sensor stromal interaction molecule 1 (STIM1) is necessary and sufficient for the store-operated Ca^{2+} entry function of transient receptor potential canonical (TRPC) 1 and 4 channels in endothelial cells. *Mol Pharmacol.* 81:510–526. https://doi.org/10.1124/mol.111.074658

Tauseef, M., V. Kini, N. Knezevic, M. Brannan, R. Ramchandaran, H. Fyrst, J. Saba, S.M. Vogel, A.B. Malik, and D. Mehta. 2008. Activation of sphingosine kinase-1 reverses the increase in lung vascular permeability through sphingosine-1-phosphate receptor signaling in endothelial cells. *Circ. Res.* 103:1164–1172. https://doi.org/10.1161/01.RES.0000338501.84810.51

Vandenbroucke, E., D. Mehta, R. Minshall, and A.B. Malik. 2008. Regulation of endothelial junctional permeability. *Ann. N. Y. Acad. Sci.* 1123:134–145. https://doi.org/10.1196/annals.1420.016

Venkatakrishnan, A.J., X. Deupi, G. Lebon, C.G. Tate, G.F. Schertler, and M.M. Babu. 2013. Molecular signatures of G-protein-coupled receptors. *Nature.* 494:185–194. https://doi.org/10.1038/nature11896

Willinger, T., S.M. Ferguson, J.P. Pereira, P. De Camilli, and R.A. Flavell. 2014. Dynamin 2-dependent endocytosis is required for sustained S1PR1 signaling. *J. Exp. Med.* 211:685–700. https://doi.org/10.1084/jem.20131343

Willinger, T., M. Staron, S.M. Ferguson, P. De Camilli, and R.A. Flavell. 2015. Dynamin 2-dependent endocytosis sustains T-cell receptor signaling and drives metabolic reprogramming in T lymphocytes. *Proc. Natl. Acad. Sci. USA.* 112:4423–4428. https://doi.org/10.1073/pnas.1504279112

Yazbeck, P., M. Tauseef, K. Kruse, M.R. Amin, R. Sheikh, S. Feske, Y. Komarova, and D. Mehta. 2017. STIM1 Phosphorylation at Y361 recruits Orai1 to STIM1 puncta and induces Ca^{2+} entry. *Sci. Rep.* 7:42758. https://doi.org/10.1038/srep42758

Zhao, Y., S.K. Kalari, P.V. Usatyuk, I. Gorshkova, D. He, T. Watkins, D.N. Brindley, C. Sun, R. Bittman, J.G. Garcia, et al. 2007. Intracellular generation of sphingosine 1-phosphate in human lung endothelial cells: Role of lipid phosphate phosphatase-1 and sphingosine kinase 1. *J. Biol. Chem.* 282:14165–14177. https://doi.org/10.1074/jbc.M701279200

Supplemental material

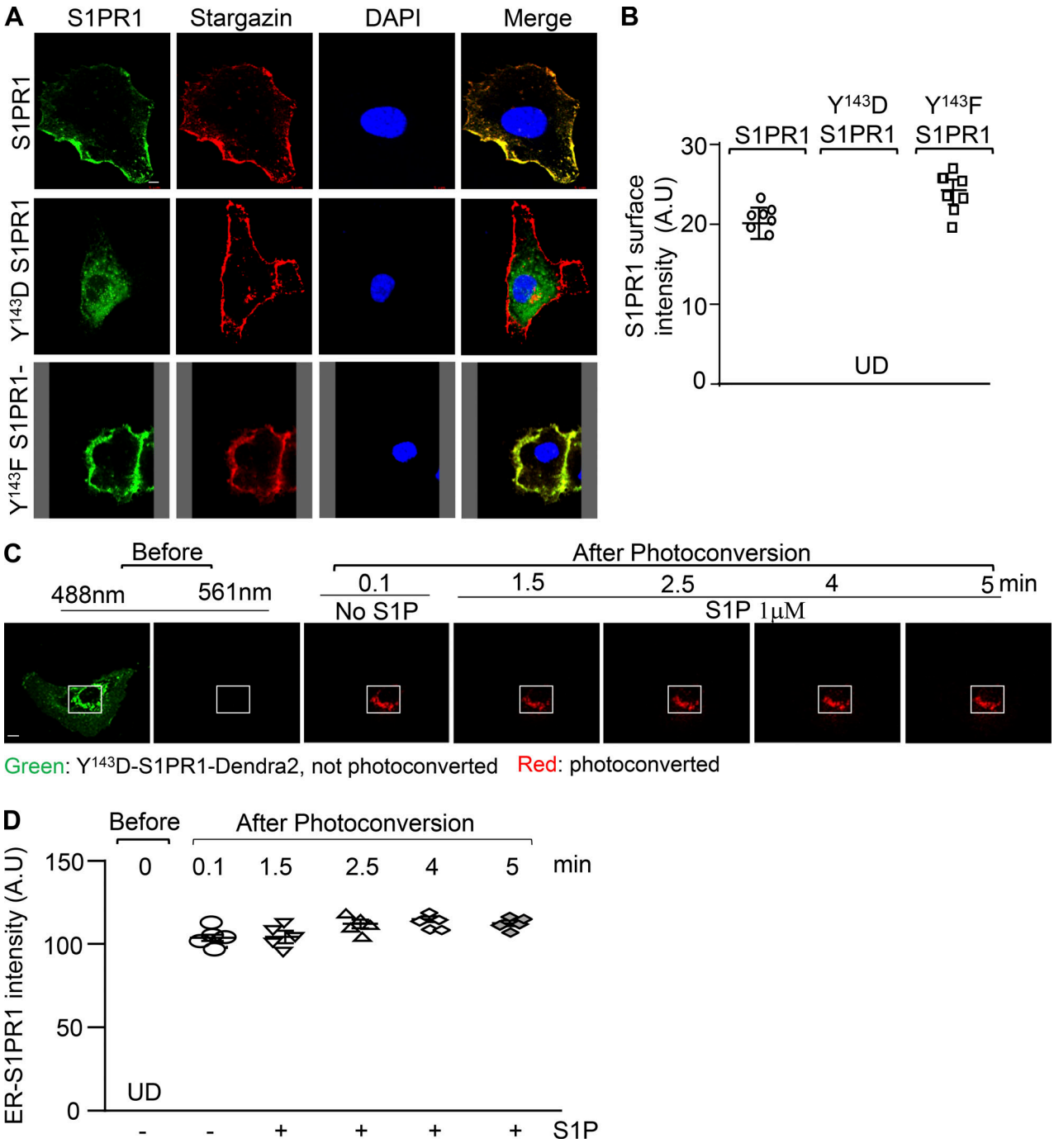

Figure S1. **S1PR1 localization. (A and B)** HUVECs coexpressing WT-S1PR1-GFP and Y^{143}D-S1PR1-GFP or Y^{143}F-S1PR1-GFP along with stargazin (membrane marker). At 24 h, cells were fixed and stained for DAPI, and images were acquired using a confocal microscope. A representative image of receptor localization in the cell is shown in A, whereas B shows the quantification of the individual data points representing receptor expression along with mean ± SD (5–8 cells/group). Scale bar, 5 µm. Gray background indicates the area outside the image. **(C and D)** Time-lapse images of Y^{143}D-S1PR1–Dendra2 before (green, rectangles) and after (red, rectangles) photoconversion at time 0 for basal (C) and after the addition of S1P (1 µM). Time is given in minutes. A representative image with time lapse of receptor localization in the cell is shown in C, while D shows the quantification of the individual data points representing receptor expression along with mean ± SD (5–6 cells). Scale bar, 10 µm. Data are from experiments that were repeated at least two times. Significance determined by one-way ANOVA followed by multiple comparisons between groups. A.U, arbitrary units; UD, undetectable.

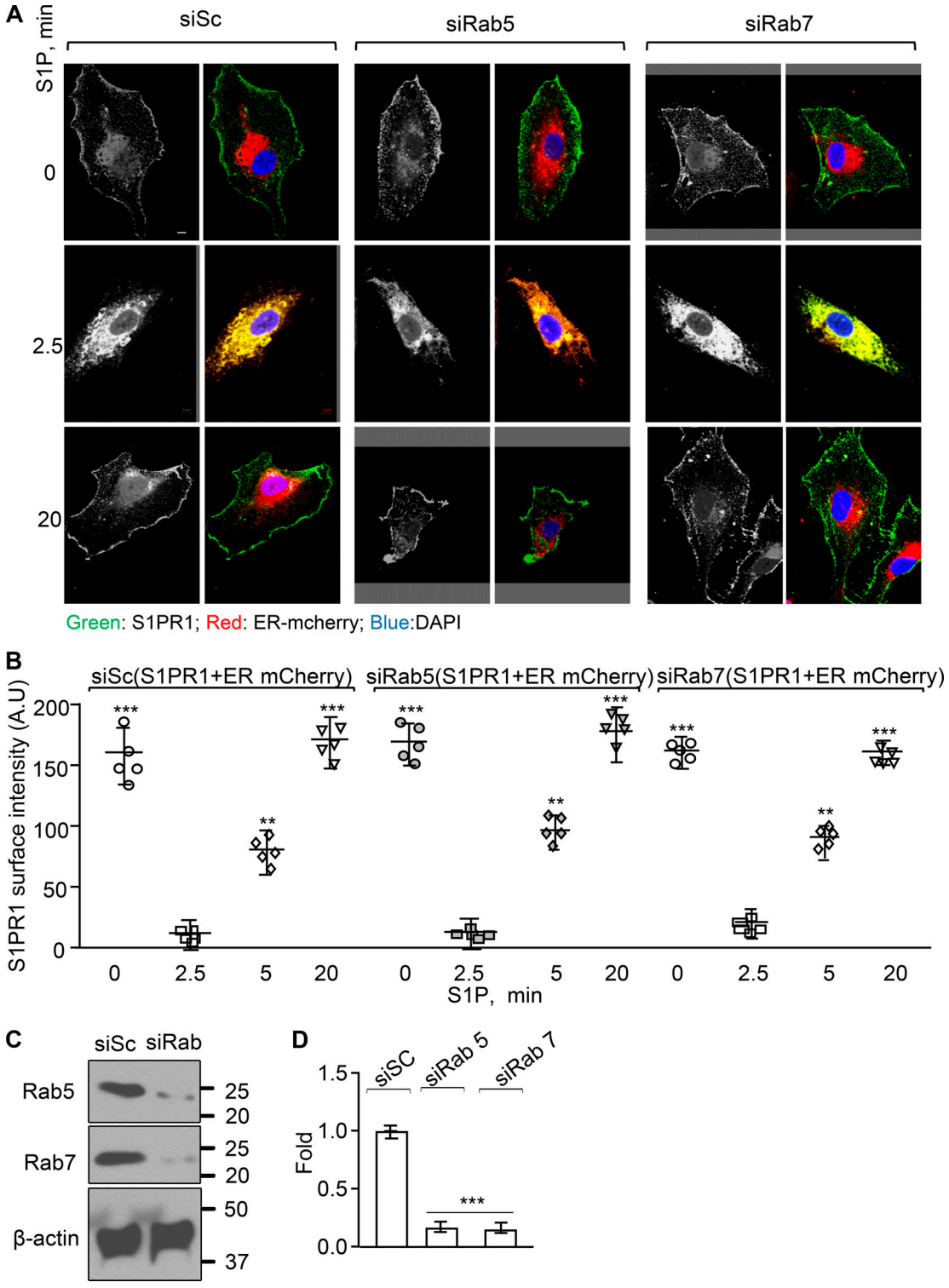

Figure S2. **S1PR1 internalizes independent of Rab-GTPases. (A and B)** HUVECs were transfected with control siRNA (siSc) or siRNA against Rab5 (siRab5) or Rab7 (siRab7) GTPases. After 24 h, cells were again cotransduced with WT-S1PR1-GFP and ER-mCherry. 48 h after transfection, cells were stimulated with S1P at the indicated time points, fixed, and stained with anti-Rab5 and anti-Rab7 antibodies followed by DAPI (nuclear stain). A shows the representative images (scale bar, 5 µm), whereas B shows the mean ± SD quantification of the surface intensity of S1PR1-GFP in HUVECs transfected with siRab5 and siRab7. n = 4–6 cells from experiments that were repeated at least two times. Gray background indicates the area outside the image. **, P < 0.001; ***, P < 0.0001 compared with S1P-stimulated siSc or siRab5 or siRab7 ECs transfected with S1PR1-GFP at 2.5 min by one-way ANOVA with two-tailed paired t test. **(C and D)** At 48 h after transfection, lysates from control or Rab5/Rab7-depleted ECs were immunoblotted using anti-Rab5 and anti-Rab7 antibodies with β-actin as a loading control. Mean ± SD Rab5 and Rab7 densities were quantified against β-actin. Blot represents experiments that were repeated multiple times independently. ***, P < 0.0001 compared with siSc-transfected ECs by one-way ANOVA with two-tailed paired t test. A.U, arbitrary units. **(C)** Molecular weight marker in kD.

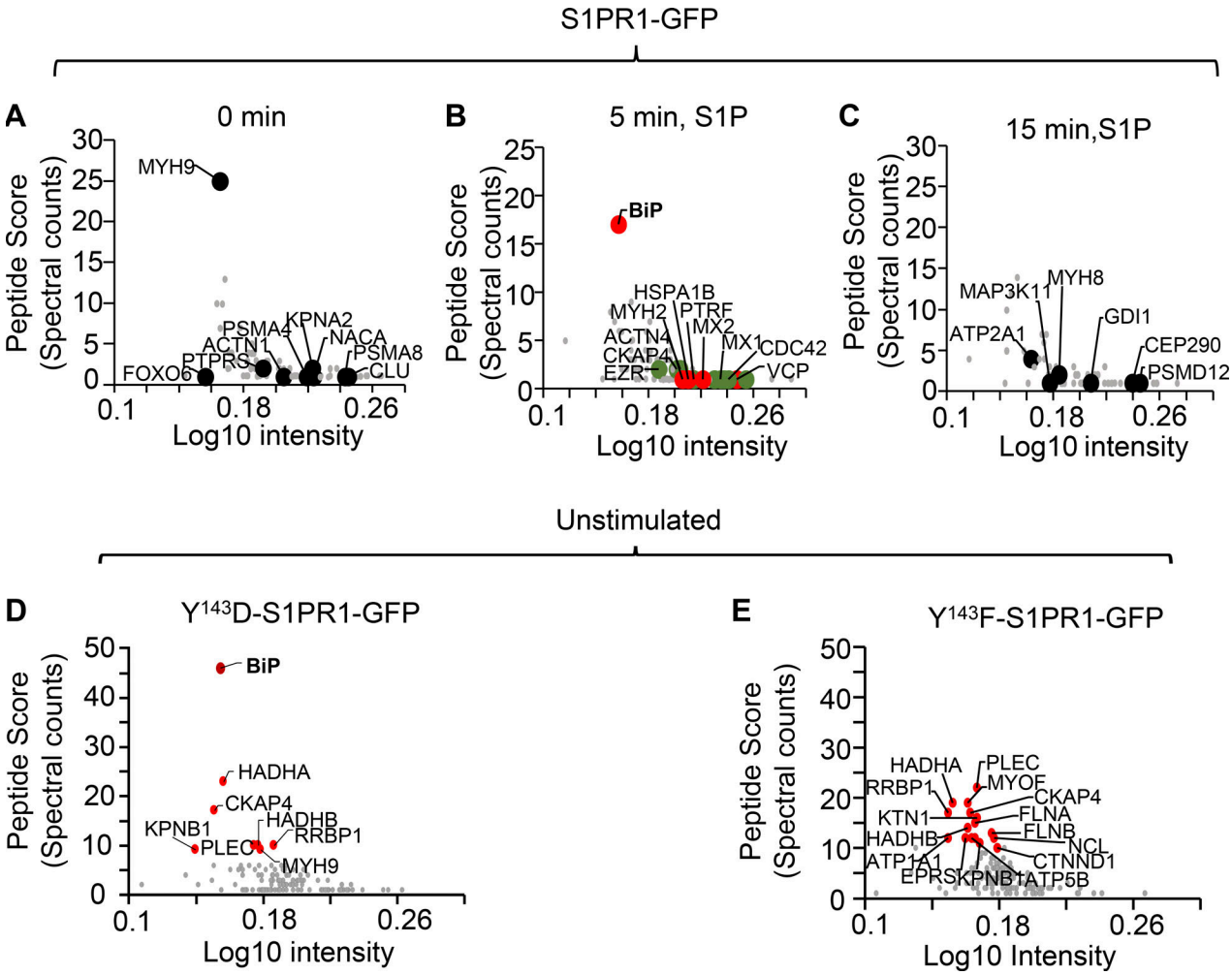

Figure S3. **Mass spectrometric analysis of S1PR1 binding partners. (A–E)** HUVECs expressing vector or GFP-tagged S1PR1, Y^{143}D-S1PR1, or Y^{143}F-S1PR1 for 24 h were either left unstimulated (A, D, and E) or stimulated with 1 µM S1P for 5 and 15 min (B and C). Lysates were immunoprecipitated using an anti-GFP antibody. Complexes were separated by SDS-PAGE and analyzed by mass spectroscopy. A scatter plot of mean intensity versus spectral counts is shown. Peptides that were overlapping with GFP were excluded from the mass spectrometry data (see Materials and methods).

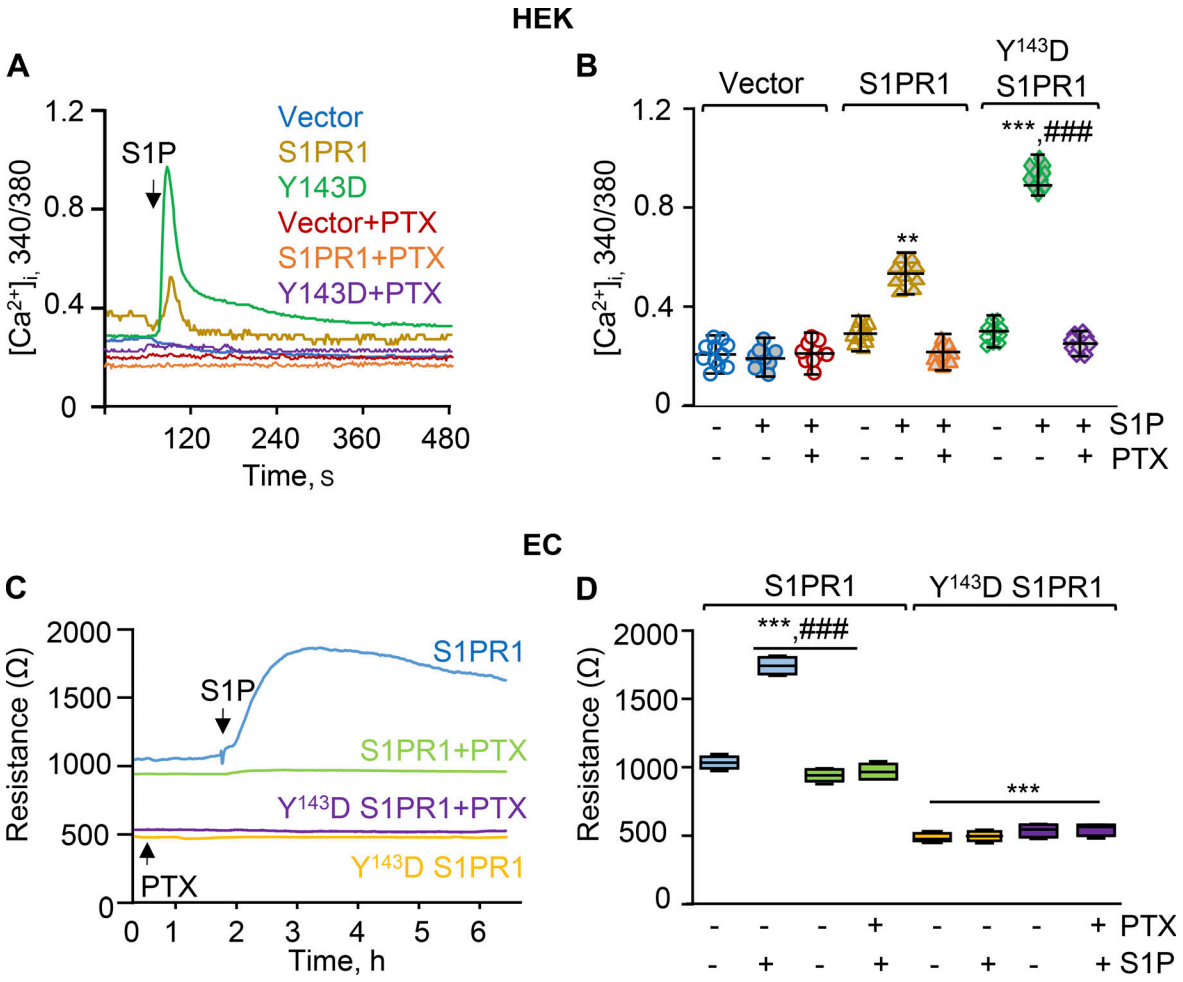

Figure S4. **Effect of inhibition of Gi on cytosolic calcium and barrier function in response to S1P. (A and B)** After 48 h after transfection, HEK cells transducing vector (GFP), GFP-tagged WT-S1PR1 or $Y^{143}D$ S1PR1 cDNAs were left untreated or pretreated with PTX (50 µM) for 2 h. Cells were then loaded with Fura-2 AM for 15 min. Ratiometric analysis of $[Ca^{2+}]_i$ was then performed after stimulation with 1 µM S1P. A shows representative traces, whereas B shows individual data points (n = 8–10 cells/group). Basal Ca^{2+} (–) was analyzed at 45 s; peak increase in Ca^{2+} was analyzed at 90 s after S1P stimulation in control or PTX-treated cells. Note that only GFP-expressing cells were chosen to assess $[Ca^{2+}]_i$ release in all experiments. **, P < 0.001; ***, P < 0.0001 compared with unstimulated cells transfected with vector or S1PR1-GFP; ###, P < 0.0001 compared with S1PR1-GFP transfected cells after S1P stimulation by one-way ANOVA with two-tailed paired t test. **(C and D)** HUVECs seeded on gold-plated electrodes were transfected with S1PR1 or $Y^{143}D$-S1PR1 cDNAs. Cells were pretreated with or without PTX (50 µM) for 2 h. TEER in real time was determined in response to 1 µM S1P. An individual TEER trace is shown in C, while D shows the quantification of the TEER from experiments that were repeated at least two times. Basal TEER in control or PTX-treated ECs was quantified as the mean between 10 and 20 min, whereas TEER after S1P addition in these ECs was calculated as the mean between 2 and 3 h. ***, P < 0.0001 compared with unstimulated cells transfected with S1PR1-GFP; ###, P < 0.0001 compared with S1PR1-GFP–transfected cells treated with PTX and S1P by one-way ANOVA with two-tailed paired t test.

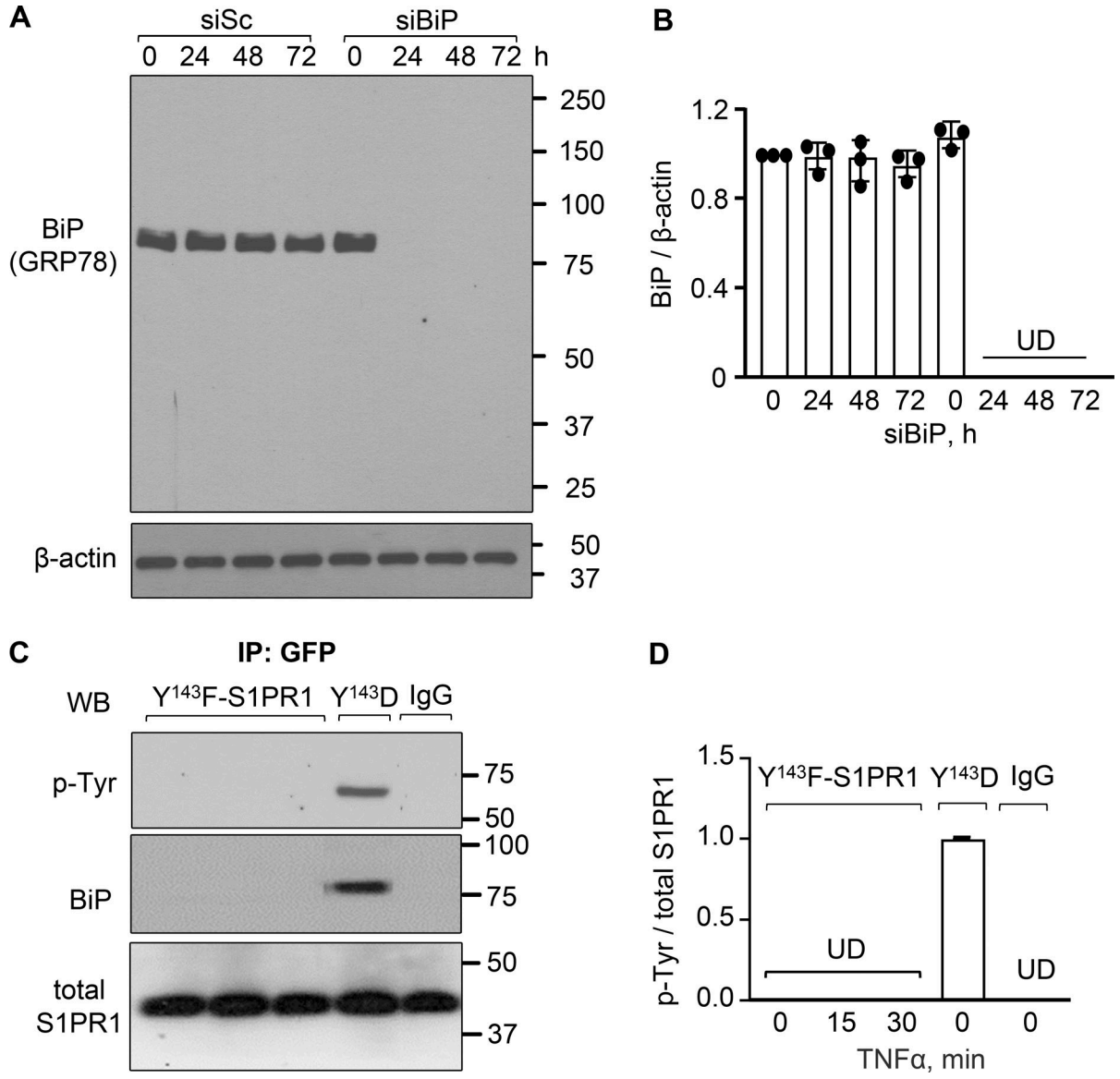

Figure S5. **TNF-α fails to phosphorylate Y^{143}F-S1PR1. (A and B)** HUVECs were transfected with control (siSc) or BiP siRNA (siBiP). Lysates were collected at the indicated times and probed for BiP and β-actin. A shows a representative blot image, whereas B shows the densitometric analysis of BiP depletion with β-actin as control. **(C and D)** HUVECs were transfected with GFP-tagged Y^{143}F-S1PR1 or Y^{143}D-S1PR1 cDNAs for 24 h, after which cells were left unstimulated or stimulated with TNF-α for 15 and 30 min in Y^{143}F-S1PR1–transducing ECs. Equal amounts of protein lysates were immunoprecipitated with anti-GFP antibody, and S1PR1 phosphorylation on Y^{143} residue and interaction with BiP was determined in immunocomplexes using anti-phosphotyrosine and anti-BiP antibodies. Lysates were probed for total S1PR1 to assess the total protein expression and loading. C shows a representative blot from experiments that were repeated at least three times, while D shows the densitometric analysis of phosphotyrosine with S1PR1 as control. Significance was determined by one-way ANOVA followed by multiple comparisons between groups. **(A and C)** Molecular weight marker in kD.